Thymic macrophages consist of two populations with distinct localization and origin

Tyng-An Zhou[1], Hsuan-Po Hsu[1], Yueh-Hua Tu[2,3], Hui-Kuei Cheng[1], Chih-Yu Lin[1], Nien-Jung Chen[1], Jin-Wu Tsai[4], Ellen A. Robey[5], Hsuan-Cheng Huang[2,6], Chia-Lin Hsu[1], and Ivan L. Dzhagalov[1*]

[1]Institute of Microbiology and Immunology, National Yang Ming Chiao Tung University, Taipei, Taiwan

[2]Bioinformatics Program, Taiwan International Graduate Program, Institute of Information Science, Academia Sinica, Taipei, Taiwan

[3]Graduate Institute of Biomedical Electronics and Bioinformatics, National Taiwan University, Taipei, Taiwan

[4]Brain Research Center, National Yang Ming Chiao Tung University, Taipei, Taiwan

[5]Division of Immunology and Pathogenesis, Department of Molecular and Cell Biology, University of California, Berkeley, CA, United States

[6]Institute of Biomedical Informatics, National Yang Ming Chiao Tung University, Taipei, Taiwan

*Correspondence to Ivan L. Dzhagalov: ivan.dzhagalov@nycu.edu.tw, ORCID: 0000-0001-9209-4582

Mailing Address: Ivan L. Dzhagalov, Institute of Microbiology and Immunology, National Yang Ming Chiao Tung University, #155, Sec. 2, LiNong Street, Beitou, Taipei City, 11221, TAIWAN

Abstract

Tissue-resident macrophages are essential to protect from pathogen invasion and maintain organ homeostasis. The ability of thymic macrophages to engulf apoptotic thymocytes is well appreciated, but little is known about their ontogeny, maintenance, and diversity. Here, we characterized the surface phenotype and transcriptional profile of these cells and defined their expression signature. Thymic macrophages were most closely related to spleen red pulp macrophages and Kupffer cells and shared the expression of the transcription factor *SpiC* with these cells. Single-cell RNA sequencing showed that the macrophages in the adult thymus are composed of two populations distinguished by the expression of *Timd4* and *Cx3cr1*. Remarkably, *Timd4*$^+$ cells were located in the cortex, while *Cx3cr1*$^+$ macrophages were restricted to the medulla and the cortico-medullary junction. Using shield chimeras, transplantation of embryonic thymuses, and genetic fate mapping, we found that the two populations have distinct origins. *Timd4*$^+$ thymic macrophages are of embryonic origin, while *Cx3cr1*$^+$ macrophages are derived from adult hematopoietic stem cells. Aging has a profound effect on the macrophages in the thymus. *Timd4*$^+$ cells underwent gradual attrition, while *Cx3cr1*$^+$ cells slowly accumulated with age and, in older mice, were the dominant macrophage population in the thymus. Altogether, our work defines the phenotype, origin, and diversity of thymic macrophages.

Introduction

Tissue-resident macrophages are present in every organ and maintain local homeostasis through diverse functions ranging from protection against pathogens to tissue repair[1]. To perform their roles efficiently, macrophages acquire specialized phenotypes depending on the tissue microenvironment, and as a consequence, multiple subtypes exist, frequently within the same organ. For example, the spleen harbors red pulp macrophages specialized in red blood cell phagocytosis, marginal zone macrophages and metallophilic macrophages that are the first defense against blood-borne pathogens, T cell zone macrophages that silently dispose of apoptotic immune cells, and tingible-body macrophages that engulf less fit B cells in the germinal center[2-4]. Thus, tissue-resident macrophages represent a fascinating developmental system that allows enormous plasticity.

The last decade has seen a paradigm shift in our understanding of the development of tissue-resident macrophages. Contrary to the long-held belief that all macrophages derive from circulating monocytes[5], multiple studies have shown that many of them are long-lived cells with an embryonic origin that can maintain themselves in the tissues (reviewed in[6]). Three waves of distinct progenitors settle the tissues and contribute in various degrees to the resident macrophages in each organ. The first wave consists of the yolk sac (YS)-derived primitive macrophages that enter all tissues and establish the earliest macrophage populations[7,8]. In all organs, except for the brain and, partially, the epidermis, primitive macrophages are replaced by the next wave consisting of fetal monocytes[9-12]. The third wave comes from hematopoietic stem cells (HSCs)-derived monocytes that contribute to various degrees to

the macrophage pool in different tissues. For example, these cells contribute little to the microglia in the brain, Langerhans cells in the epidermis, and alveolar macrophages in the lungs but substantially to most other organs[13-16]. Moreover, the kinetics and timing of HSC-derived monocyte infiltration vary in different parts of the body. For some macrophage populations, such as the arterial macrophages and subcapsular lymph node macrophages, monocytes replace embryonic macrophages soon after birth and self-maintain after that with little contribution from circulating cells[17,18]. Others, such as heart macrophages, osteoclasts, and pancreatic islets macrophages, are progressively replaced at a low rate[14,19-23]. A third group, such as the macrophages in the dermis and most of the gut macrophages, are constantly replaced by blood monocytes with relatively fast kinetics[24,25]. These conclusions have been extended to many different macrophage populations such as Kupffer cells, liver capsular macrophages, red pulp macrophages, testicular macrophages, large and small peritoneal macrophages, and T zone macrophages in the lymph nodes[2,13,14,16,26-30].

The recent revitalization in macrophage research has yet to reach thymic macrophages. Although their prodigious phagocytic ability is well appreciated[31], little is known about the origin, diversity, and maintenance of these cells. This gap in our knowledge is, partly, due to the lack of a consensus about the surface phenotype of thymic macrophages. Various groups have used different markers to identify these cells, such as F4/80 and Mac-3 (LAMP-2)[31], or CD4 and CD11b[32], or Mac-2 (galectin 3), F4/80 and ED-1 (CD68)[33]. Most commonly, researchers employ F4/80 and CD11b[34-37]. However, none of these markers is macrophage-specific: F4/80 is also

expressed on eosinophils and monocytes[38,39], while CD11b is present on most myeloid cells. The lack of a clear phenotypic definition of thymic macrophages has translated into the absence of models that target genes specifically in this population. For example, although macrophages in various organs have been successfully targeted with *Lyz2*^{Cre}, *Csf1r*^{Cre}, or *Cx3cr1*^{Cre}, very few studies have used these models in the thymus[37,40,41].

Only a handful of studies have explored the origin of thymic macrophages. Several reports have indicated that these cells could be derived from T cell progenitors in the thymus based on an improved single cell in vitro culture and in vivo transplantation experiments[42,43]. However, these conclusions have been questioned based on fate-mapping experiments using *Il7r*^{Cre} that found very limited contribution of lymphoid progenitors to thymic macrophages in vivo in unperturbed mice[44]. Most recently, Tacke et al. used parabiosis to rule out circulating monocytes as a major source of thymic macrophages[37]. The same study also performed fate-mapping experiments to show that most thymic macrophages descend from *Flt3*$^{+}$ HSC-derived progenitors. However, the contribution of earlier waves of hematopoiesis has not been explored.

Here, we aimed to bring our knowledge of thymic macrophages on par with other tissue-resident macrophages. We started by clearly defining thymic macrophages according to the guidelines set by the Immunological Genome Consortium (IMMGEN)[38] and characterized their surface phenotype and transcriptional signature. Using single-cell RNA sequencing (scRNA-Seq), we identified two populations of thymic macrophages with distinct localization. We explored the origin of these cells through genetic fate mapping, shield chimeras, and embryonic thymus transplantation and documented that

different waves of progenitors give rise to the two populations of thymic macrophages. Altogether our work fills an important gap in our understanding of resident thymic macrophages and provides the framework for future functional characterization of these cells.

Results:

CD64, F4/80, and MerTK identify the macrophages in the thymus

To unambiguously and comprehensively identify macrophages in the thymus, we evaluated several of the prototypical macrophage markers – MerTK, CD64, and F4/80[38]. A population that was stained with all three markers (Figure 1A). As staining with MerTK and F4/80 was relatively dim even when the brightest fluorochromes (e.g., PE) were used and could not be resolved fully from the isotype control (Figure 1 – figure supplement 1), we chose to use CD64 vs. forward scatter (FSC) as the first step in our gating strategy (Figure 1B). Among $CD64^{+}FSC^{hi}$ cells, $F4/80^{+}CD11b^{lo}$ macrophages could be distinguished from $F4/80^{lo}CD11b^{+}$ monocytes.

The $CD64^{+}F4/80^{+}MerTK^{+}CD11b^{lo}FSC^{hi}$ cells had typical macrophage morphology with abundant cytoplasm (Figure 1C). These cells did not express lineage markers characteristic of T cells (CD3ε), B cells (CD19), eosinophils (Siglec F), NK cells (NK1.1), neutrophils (Gr1), or plasmacytoid dendritic cells (Siglec H) (Figure 1D). However, they expressed phagocytic receptors such as TIM4, CD51, and Axl (Figure 1E). Immunofluorescent staining with CD64, MerTK, and TIM4 in the thymic cortex confirmed the presence of large cells positive for all three macrophage markers (Figure 1 – figure supplement 2).

To ascertain that our gating strategy identifies all macrophages in the thymus in an unbiased way, we performed scRNA-Seq of sorted *Csf1r*$^{GFP+}$ and *Cd11c*$^{YFP+}$ thymic cells. *Csf1r* is required for the survival of most macrophages and is considered their definitive marker[45,46], while *Cd11c*^{YFP} is expressed in many myeloid cells, including macrophages[47]. Both reporters identified an overlapping set of cells (Figure 1 – figure supplement 3). Two clusters expressed the macrophage/monocytes-specific transcription factor *Mafb* and high levels of *Fcrg1* (CD64), *Mertk*, and *Adgre1* (F4/80), indicating that they are macrophages (Figure 1F). An additional cluster expressed *Mafb* together with *Fcgr1* and *Adgre1* but not *Mertk*, fitting the description of monocytes. Altogether the scRNA-Seq data confirmed that our flow cytometry gating had identified all macrophages in the thymus. Importantly, MerTK^{+} cells could not be labeled by intravenously injected CD45 antibody (Figure 1G), proving that they reside in the parenchyma of the organs and not in the blood vessels. Based on the above data, we will refer to CD64^{+}F4/80^{+}MerTK^{+}CD11b^{lo}FSC^{hi} cells as thymic macrophages. The smaller CD64^{+}F4/80^{lo}CD11b^{+}FSC^{hi} population did not express MerTK but most of them expressed Ly6C, and we classified them as thymic monocytes.

Thymic macrophages expressed CD11c, MHC2, and SIRPα making them partially overlap with CD11c^{+}MHC2^{+} classical dendritic cells (cDCs), thus making problematic the unambiguous identification of thymic cDCs based only on these two markers (Figure 1 – figure supplement 4). Proper identification of cDC in the thymus requires the exclusion of macrophages based on CD64 or MerTK staining. Otherwise, the cDCs, particularly the SIRPα^{+} cDC2 subset,

would be contaminated with macrophages that account for ~25% of cDC2 (Figure 1 – figure supplement 5).

Thymic macrophages were ~0.1% of all the cells in the thymus of young adult mice and numbered ~4x10^5 on average per mouse (Figure 1H). We did not find statistically significant differences in their percentages between 4 and 11 weeks of age. Still, there was a significant decline in their numbers with age, consistent with the beginning of thymic involution (Figure 1I).

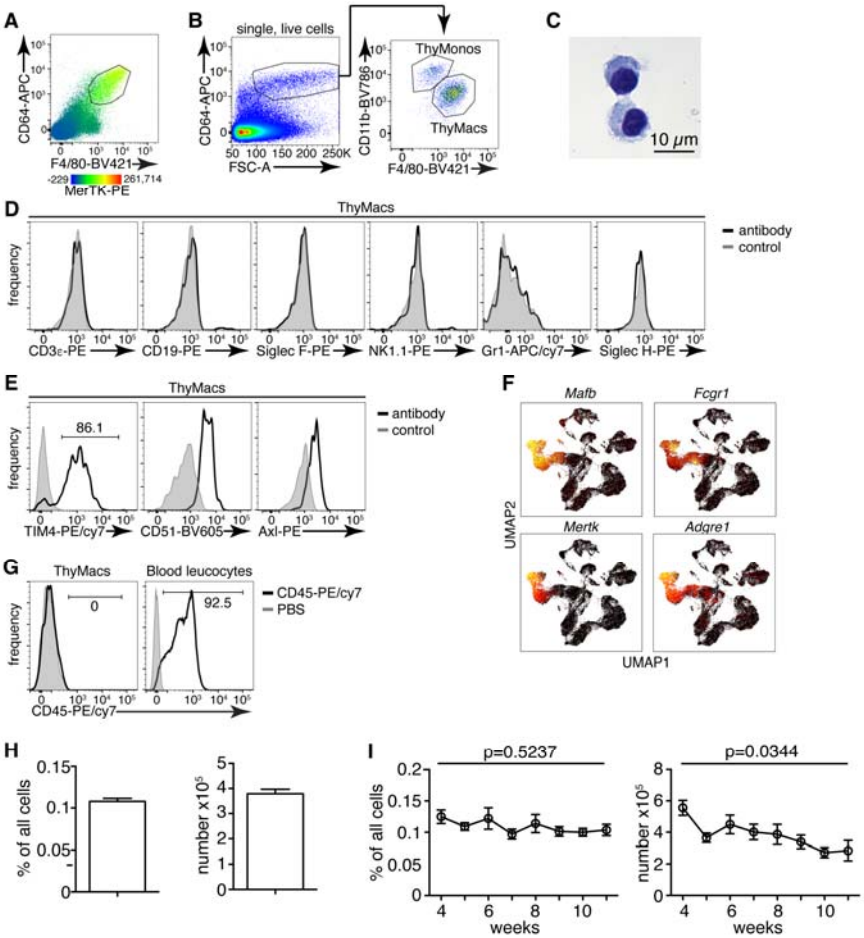

Figure 1. Thymic macrophages (ThyMacs) can be identified by the expression of CD64, MerTK, and F4/80. A Flow cytometric analysis of enzymatically digested thymus tissue with macrophage markers CD64, MerTK, F4/80, and CD11b. **B** Gating strategy for identifying thymic

macrophages: CD64^{+}FSC^{hi} are first gated; the F4/80^{+}CD11b^{lo} cells among them are the thymic macrophages (ThyMacs), while F4/80^{lo}CD11b^{+} are the thymic monocytes (ThyMonos). **C** Pappenheim (Hemacolor Rapid staining kit) staining of sorted ThyMacs. **D** Lack of expression of lineage markers associated with other cell types on ThyMacs. **E** The expression on ThyMacs of three receptors for phosphatidylserine that participate in the phagocytosis of apoptotic cells. **F** scRNA-Seq data showing the expression of prototypical macrophage genes *Mafb*, *Fcgr1* (CD64), *Mertk*, and *Adgre1* (F4/80) among thymus cells sorted as *Csf1r*$^{GFP+}$ and *Cd11c*$^{YFP+}$. **G** Labeling of ThyMacs with intravenously injected anti-CD45-PE antibody or PBS. The labeling of blood leucocytes is shown for comparison. **H** Average numbers and percentages of ThyMacs in 4-11 weeks old mice, n=82. **I** Comparison of the numbers and percentages of ThyMacs in mice of different ages, n=82. All flow cytometry plots are representative of at least 3 independent repeats. The numbers in the flow cytometry plots are the percent of cells in the respective gates. Data in **H** and **I** represent mean±SEM. Statistical significance in **I** was determined with one-way ANOVA.

Transcriptional signature of thymic macrophages

To further understand the identity and functions of the thymic macrophages, we analyzed the RNA sequencing data from the IMMGEN's Open Source Mononuclear Phagocyte profiling. We first examined the expression of the core signature macrophage genes[38] and found that they were enriched in thymic macrophages but not in *Sirpa*$^{+}$ or *Xcr1*$^{+}$ thymic cDCs (Figure 2A). On the contrary, cDC core signature genes were abundantly

expressed in both thymic cDC subsets but not in thymic macrophages. Thus, although thymic macrophages and cDCs share the thymic microenvironment and expression of CD11c and MHC2, they have distinct transcriptional profiles.

We then compared the gene expression profile of thymic macrophages to that of other well-characterized macrophage populations from the IMMGEN database. Because of the abundance of samples, we limited our comparison to only nine types of tissue-resident macrophages under steady-state conditions – splenic red pulp macrophages, Kupffer cells, broncho-alveolar lavage macrophages, large peritoneal cavity macrophages, white adipose tissue macrophages, aorta macrophages, central nervous system microglia, and spinal cord microglia. Principal component analysis revealed that thymic macrophages were most closely related to splenic red pulp macrophages and Kupffer cells (Figure 2B).

To better identify the unique functions of thymic macrophages, we looked for differentially expressed genes in these cells compared to other tissue-resident macrophages. We set three criteria: 1) high expression in thymic macrophages (>500); 2) >5-fold higher expression than the average value in the nine populations of non-thymic macrophages; 3) expression in thymic macrophages is higher than any non-thymic macrophage samples. A total of 44 genes met these criteria, and we consider them to constitute the transcriptional signature of thymic macrophages (Figure 2C). These included several degradation enzymes and their inhibitors (*Cst7*, *Mmp2*, *Mmp14*, *Dnase1l3*, *Serpina3g*, *Acp5*), non-classical MHC molecules (*H2-M2*, *H2-Q6*, *H2-Q7*), metabolic enzymes (*Chst2*, *Ass1*, *Kynu*, *Cp*, *Dgat2*, *Sorl1*, *Lap3*),

molecules involved in innate immunity (*Ifit2*, *Il18bp*, *Mefv*, *Lgals3bp*) and extracellular signaling molecules and their receptors (*Pdgfa*, *Cxcl16*, *Il2rg*, *Gpr157*). We also looked for transcription factors (TFs) highly expressed in thymic macrophages and could potentially regulate critical gene networks in these cells. A total of 25 TFs were highly expressed in thymic macrophages (>250) and were at least 2-fold higher as compared to the non-thymic macrophages (Table 1). Among them were several TFs involved in type I interferon (IFN-I) signaling (*Stat1*, *Stat2*, *Irf7*, and *Irf8*) and lipid metabolism (*Nr1h3*, *Pparg*, *Srebf1*, and *Rxra*) (Figure 2D). Notably, *Runx3*, which is essential for the development and function of cytotoxic T lymphocytes[48], innate lymphoid cells[49], and Langerhans cells[50], was highly expressed in thymic macrophages. *SpiC*, which has well-documented roles in the development of red pulp macrophages in the spleen and bone marrow macrophages[51,52], was also highly expressed in thymic macrophages, further strengthening the argument for the similarity between thymus, spleen, and liver macrophages. To confirm the expression of *Spic* in thymic macrophages, we analyzed the thymus of *Spic*^{GFP} mice[52]. We found that all *Spic*$^{GFP+}$ cells were macrophages (Figure 2 – figure supplement 1), making them the most specific thymic macrophage reporter strain compared with *Lyz2*^{GFP}, MAFIA (*Csf1r*^{GFP}), *Cd11c*^{YFP}, and *Cx3cr1*^{GFP} mice (Figure 2 – figure supplement 2). However, only ~80% of thymic macrophages were *Spic*$^{GFP+}$ suggesting heterogeneity within the cells (Figure 2 – figure supplement 3).

Several dominant pathways emerged when we grouped the 500 most highly expressed genes in thymic macrophages according to gene ontology (GO) terms (Figure 2E). Notably, five of the ten most highly enriched GO

pathways concerned antigen presentation of both exogenous and endogenous antigens. These data complement our flow cytometry findings of expression of MHC2 and suggest that thymic macrophages could be potent antigen-presenting cells and might play a role in negative selection or agonist selection of thymocytes. Two other highly enriched GO pathways were involved in lysosomal biogenesis and functions, highlighting the high capacity of these cells to degrade phagocytosed material. Thus, our transcriptional analysis has revealed that thymic macrophages are bona fide macrophages that bear significant similarity to spleen and liver macrophages and are specialized in lysosomal degradation of phagocytosed material and antigen presentation.

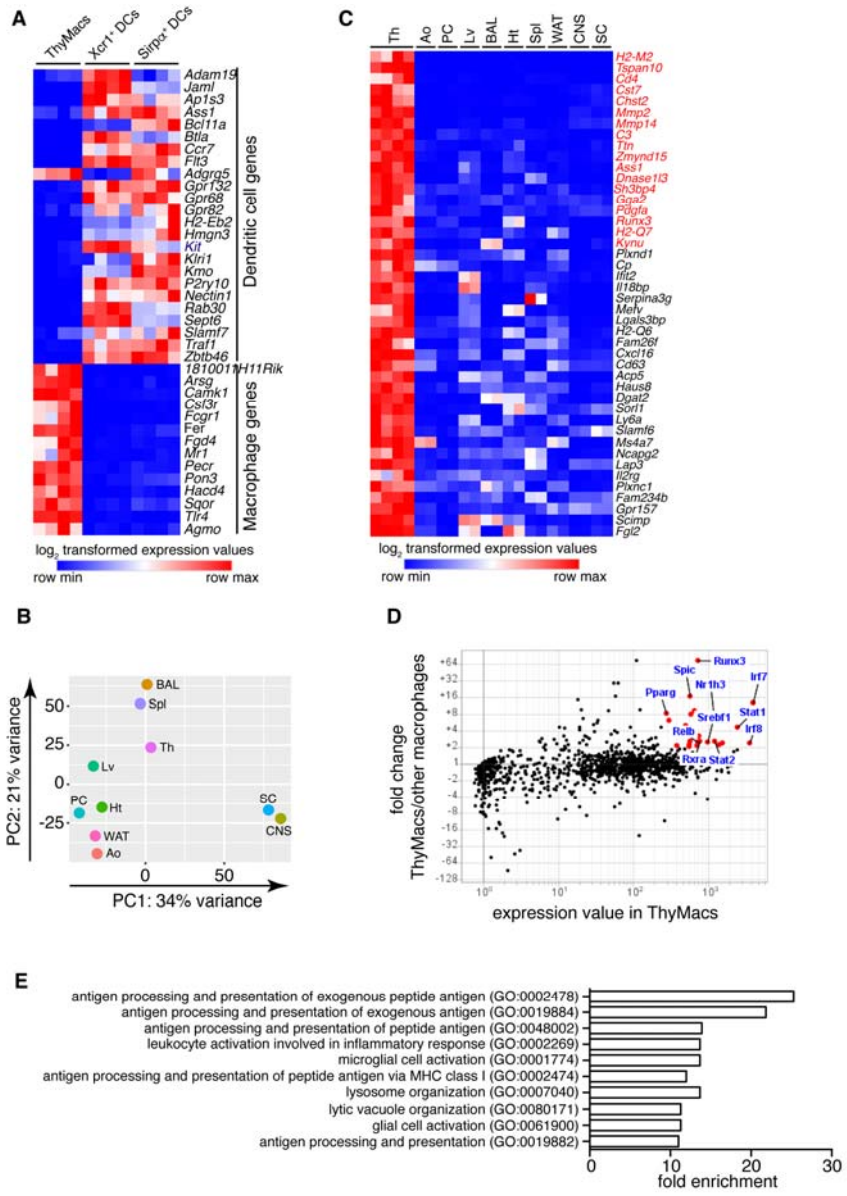

Figure 2. Transcriptional profile of thymic macrophages (ThyMacs). A Expression of cDC-specific genes (top) and macrophage-specific genes (bottom) in ThyMacs and two populations of thymic cDCs (ThyDCs) – *Xcr1*$^{+}$ ThyDCs and *Sirpa*$^{+}$ ThyDCs. **B** Principal components analysis of ThyMacs and nine other populations of tissue-resident macrophages in duplicates. **C** Highly expressed (>500) genes enriched (>5-fold) in ThyMacs (4 samples) compared to nine other tissue-resident macrophage populations (two samples each). The genes in red are >10-fold up-regulated in thymic macrophages. **D**

Comparison of the geometric mean expression of transcription factors in thymic macrophages (4 samples) and the nine other macrophage populations (2 samples each). Transcription factors with expression >250 and fold change >2 are marked with red dots. **E** Top 10 GO pathways in ThyMacs based on the 500 most highly expressed genes in these cells. Th – ThyMacs, Spl – spleen red pulp macrophages, Lv – Kupffer cells, BAL – broncho-alveolar lavage macrophages, PC – peritoneal cavity macrophages, Ao – aorta macrophages, Ht – heart macrophages, WAT – white adipose tissue macrophages, CNS – central nervous system microglia, SC – spinal cord microglia.

Thymic macrophages can present antigens to T cells and clear apoptotic cells

Next, we investigated the biological functions of thymic macrophages. Our findings that these cells express MHC2 and many other genes involved in antigen presentations prompted us to test if they can efficiently activate T cells. We pulsed sorted thymic macrophages with chicken ovalbumin (Ova) and cultured them with naïve OT2 cells labeled with CFSE. The positive control, thymic DCs, efficiently induced OT2 cell proliferation, while peritoneal macrophages were very inefficient (Figure 3A and B), similar to other tissue-resident macrophages[2]. Surprisingly, thymic macrophages induced proliferation in a considerable proportion (~30%) of OT2 cells as calculated by FlowJo's Proliferation Modeling module. Thus, thymic macrophages are able antigen-presenting cells, although not as good as DCs.

To confirm the ability of thymic macrophages to clear apoptotic cells, we did in vitro engulfment assay. Thymocytes were induced to undergo apoptosis by Dexamethasone treatment and labeled with pHrodo Red dye. pHrodo Red is weakly fluorescent at neutral pH, but its fluorescence increases significantly at low pH, for example, in lysosomes. Thus, engulfed apoptotic cells can be clearly identified by their strong red fluorescence. We incubated the pHrodo Red-labeled apoptotic thymocytes for 2 hours with sorted thymic or peritoneal cavity macrophages and detected the extent of efferocytosis by fluorescent microscopy. Thymic macrophages were avid phagocytes, and we could record many instances of efferocytosis at this time point (Figure 3C and D). However, peritoneal macrophages were able to phagocytose even more apoptotic cells.

To determine if thymic macrophages are the major phagocytes in the thymus in vivo, we evaluated their participation in the phagocytosis of apoptotic cells in the thymus by TUNEL staining. Most TUNEL$^+$ cells could be found clearly inside or closely associated with MerTK$^+$ and TIM4$^+$ cells in the thymus (Figure 3E and F). On average, ~85% of all TUNEL$^+$ cells were within 5 µm of MerTK$^+$ cells, confirming that thymic macrophages are the dominant phagocytic population in the thymus (Figure 3G). The degree of co-localization between TUNEL$^+$ cells and TIM4$^+$ cells was slightly lower, ~75% on average, possibly reflecting the absence of TIM4 expression on a small proportion of thymic macrophages (Figure 1E).

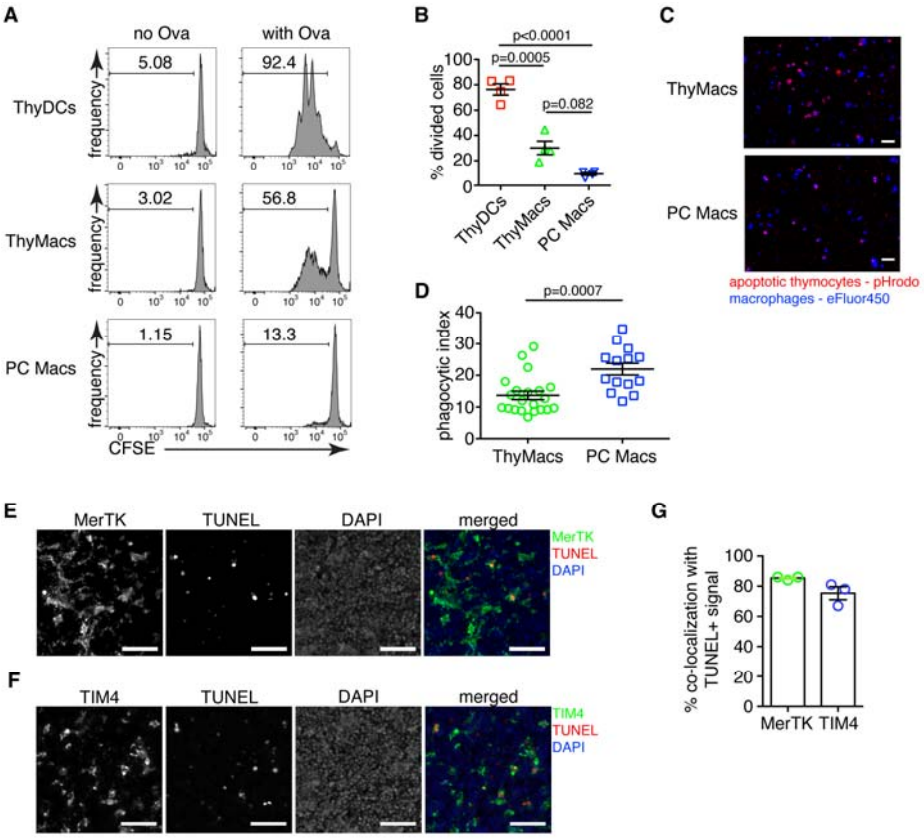

Figure 3. Thymic macrophages can present antigens to T cells and phagocytose apoptotic cells. A Naïve OT2 T cells were labeled with CFSE and cultured with purified thymic dendritic cells (ThyDCs), thymic macrophages (ThyMacs), or peritoneal cavity macrophages (PC Macs) in the presence or absence of chicken ovalbumin (Ova). Three days later, the CFSE dilution was assessed by flow cytometry. **B** Quantification of the cell division in naïve OT2 cells by using the Cell Proliferation module in FlowJo that calculates the percent of cells from the initial population that has undergone division. **C** Example immunofluorescent images of ThyMacs or PC Macs phagocytosis apoptotic thymocytes. The macrophages were labeled with eFluor 450, while the apoptotic thymocytes – with pHrodo Red. An intense red signal within the macrophages indicates phagocytosed thymocytes. **D** Quantification of the percentage of macrophages that have engulfed at least

one thymocyte (phagocytic index). **E** Example images showing co-localization of TUNEL$^+$ apoptotic cells and MerTK$^+$ ThyMacs in thymic sections. **F** Example images showing co-localization of TUNEL$^+$ apoptotic cells and TIM4$^+$ ThyMacs in thymic sections. Scale bars in **E** and **F** are 50 µm. **G** Frequencies of the co-localization of TUNEL$^+$ signal with MerTK$^+$ and TIM4$^+$ cells. Flow cytometry plots in **A** are representative of three independent experiments. All immunofluorescent images are representative of at least 3 independent repeats. Data in **B**, **D**, and **G** represent mean±SEM. Each symbol in **B** and **G** is an individual mouse. Each symbol in **D** is a field of view.

Expression of *Timd4* and *Cx3cr1 can distinguish* two populations of thymic macrophages

Our phenotypic characterization showed clear signs of heterogeneity within thymic macrophages, including the presence of TIM4$^+$ and TIM4$^-$ cells (Figure 1E) and *Cx3cr1*$^{GFP+}$ and *Cx3cr1*$^{GFP-}$ cells (Figure 2 – figure supplement). To determine the degree of thymic macrophage heterogeneity, we turned to our scRNA-Seq data. At least 7 clusters could be identified and assigned to different cell types by specific marker expression (Figure 4A and B), including macrophages, B cells, pDCs, contaminating thymocytes, and multiple cDC clusters. Once we zoomed onto *Mafb*-expressing cells, we could distinguish three separate populations: 1) monocytes that expressed high levels of *Ly6c2* and *Itgam* (CD11b) but did not express *Mertk*; 2) *Timd4*$^+$ (encoding TIM4) macrophages that also expressed high levels of *Spic* and *Slc40a1*, but low levels of *Cx3cr1*; 3) *Cx3cr1*$^+$ macrophages that expressed low levels of *Timd4*, *Spic*, and *Slc40a1* (Figure 4C and D). Both macrophages and

monocytes expressed *Fcgr1* (CD64). Thus, these data indicate that thymic macrophages consist of two populations with distinct expression profiles.

We confirmed the results from scRNA-Seq by flow cytometry. We could identify discrete TIM4^{+}*Cx3cr1*$^{GFP-}$ and TIM4^{-}*Cx3cr1*$^{GFP+}$ macrophages (Figure 4E). There was even a TIM4^{+}*Cx3cr1*$^{GFP+}$ intermediate population that could not be distinguished in the scRNA-Seq dataset, likely because of the lack of statistical power. To determine the localization of the two distinct macrophage populations, we stained thymic sections from *Cx3cr1*^{GFP} mice with an antibody to MerTK. The *Cx3cr1*$^{GFP-}$ MerTK^{+} cells correspond to *Timd4*$^{+}$ macrophages, while the *Cx3cr1*$^{GFP+}$MerTK^{+} cells would be the *Cx3cr1*$^{GFP+}$ macrophages. Strikingly, the two macrophage populations showed distinct localization in young mice. *Timd4*$^{+}$ macrophages were located in the cortex, while the *Cx3cr1*$^{GFP+}$ macrophages resided in the medulla and the cortico-medullary junction (Figure 4F). The result was confirmed with direct staining for TIM4 that showed intense signal in the cortex, particularly in the deep cortex, and absence of staining in the medulla (Figure 4 figure supplement 1). However, the medulla still featured many CD64^{+} macrophages.

To better understand the differences between the two populations of thymic macrophages, we looked for differentially expressed genes. We included the thymic monocytes in the comparison, as these cells clustered the closest to macrophages. *Timd4*$^{+}$ macrophages expressed the highest levels of the transcription factors *Spic*, *Maf*, and *Nr1h3*; the receptors for apoptotic cells *Axl*, *Mertk*, and *Timd4*; and many Slc transporters such as *Slc40a1*, *Slc1a3*, *Slco2b1*, *Slc11a1*, and *Slc7a7* (Figure 4G and Table 2). *Cx3cr1*$^{+}$ macrophages expressed high levels of the transcription factor *Runx3*; a

distinct set of phosphatidylserine receptors such as *Stab1*, *Anxa5*, and *Anxa3*; many degradative enzymes such as *Mmp2*, *Mmp14*, *Dnase1l3*, *Acp5*, *Lyz2*, *Ctsz*, *Ctss*, *Ctsd*, *Ctsl*; cytokines such as *Pdgfa*, *Cxcl16*, and *Ccl12*; and molecules involved in MHC1 antigen presentation such as *B2m*, *H2-M2*, *H2-K1*, *H2-Q7*. Thymic monocytes were characterized by differential expression of the typical monocyte genes *Ly6c2*, *Ccr2*, and *S100a4*, and genes involved in MHC2 antigen presentation such as *Ciita*, *H2-DMb1*, *H2-Ab1*, and *Cd74*.

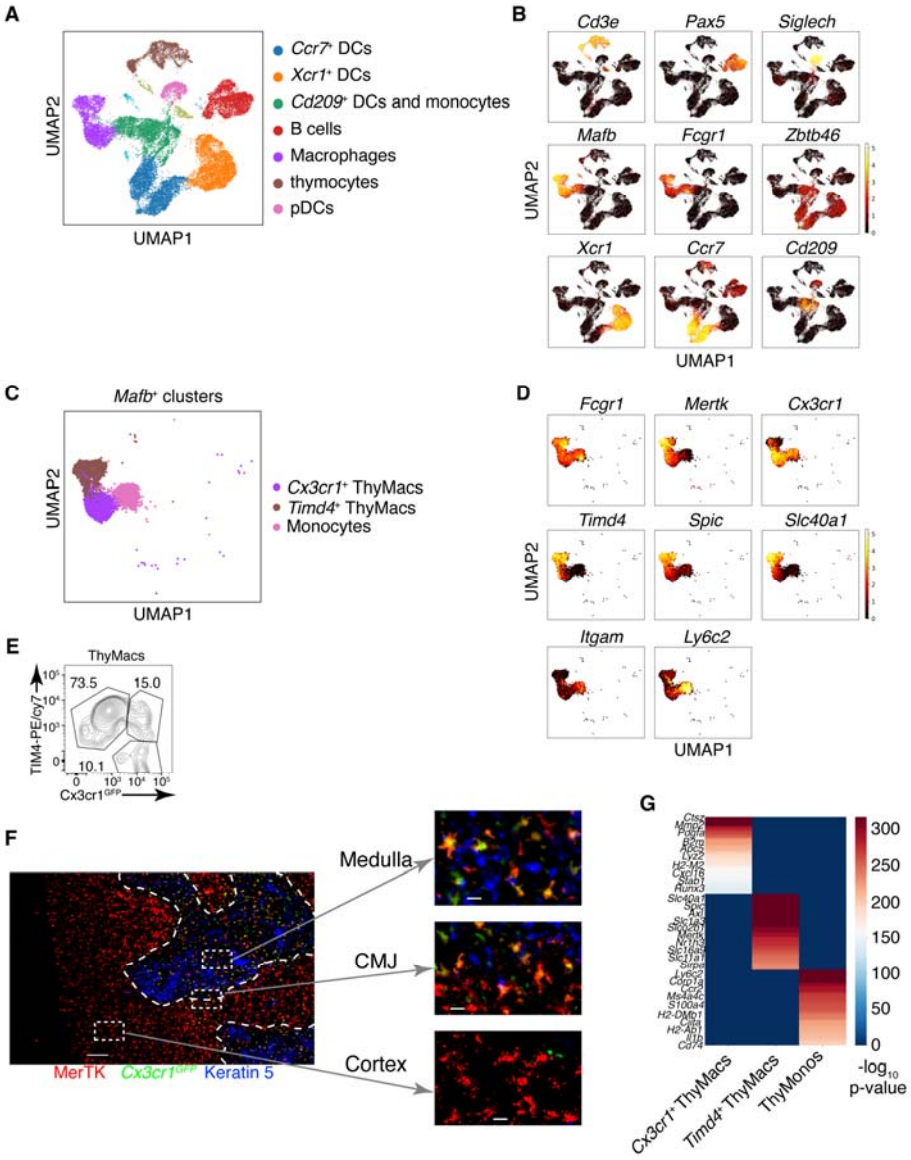

Figure 4: **Two populations of macrophages with distinct localization exist in the thymus. A** Identification of the clusters from the scRNA-Seq data based on lineage-specific markers. **B** Expression of lineage-specific markers in different clusters. **C** UMAP clusters from **A** with high expression of the transcription factor *Mafb* fall into three groups: monocytes, *Timd4*$^{+}$ macrophages, and *Cx3cr1*$^{+}$ macrophages. **D** Expression of the indicated genes in the three *Mafb*-positive clusters. **E** A flow cytometry plot of *Cx3cr1*^{GFP} and TIM4 expression in ThyMacs. The plot is representative of >10 individual experiments. The numbers inside the plot are the percentages of the cell populations in the respective gates. **F** Immunofluorescent staining of the thymus of *Cx3cr1*^{GFP} mouse stained with MerTK (a marker for all macrophages) and Keratin 5 (a marker for medulla). The scale bar is 150 µm. Areas in the cortex, medulla, and the cortico-medullary junction (CMJ) represented by the dashed boxes are enlarged to the right to show the co-localization of *Cx3cr11*^{GFP} and MerTK signal in CMJ and medulla, but not in the cortex. The scale bars in the images to the right are 20 µm. The images are representative of three individual mice. **G** Differentially expressed genes among *Timd4*$^{+}$ thymic macrophages, *Cx3cr1*$^{+}$ thymic macrophages, and thymic monocytes. The negative $\log_{10}$ p-values for the genes expressed in each cluster were calculated as described in the Materials and Methods, and the top 50 differentially expressed genes were plotted in the figure. Ten of these genes are listed on the left.

Yolk-sac progenitors contribute to embryonic thymic macrophages

The ontogeny of thymic macrophages has been examined by only one study since the realization that many tissue-resident macrophages are descendants of embryonic progenitors[37]. Based on *Flt3*^{Cre} fate-mapping, the authors concluded that most adult thymic macrophages derive from HSCs. To determine if yolk-sac (YS) progenitors contribute to embryonic thymic macrophages, we used *Cx3cr1*^{CreER} fate mapping[53]. Injection of 4-OHT at E9.5 in *ROSA26*$^{LSL\text{-}GFP}$ mouse mated with a *Cx3cr1*^{CreER} male permanently tags YS progenitors and their descendants with GFP (Figure 5A). Indeed, E19.5 microglia that are exclusively derived from YS progenitors were labeled to a high degree (Figure 5B). After adjusting for incomplete labeling based on the microglia, we found that at E15.5 >50% of thymic macrophages were fate mapped, i. e. from YS origin (Figure 5C). However, GFP^{+} thymic macrophages decreased to just ~11% at E19.5, suggesting that YS progenitors establish the embryonic thymic macrophage pool but are quickly replaced by subsequent wave(s) of macrophages.

Differential contribution of adult bone marrow-derived monocytes to the two thymic macrophage populations

To investigate the possibility that thymic macrophages arise from adult bone marrow-derived monocytes, we devised two complementary experiments. First, we evaluated the contribution of circulating adult monocytes to thymic macrophages without the confounding effect of radiation damage on the thymus. We created shield chimeras by subjecting CD45.2 mice to a lethal dose of irradiation while protecting their upper body and the thymus with a 5 cm lead shield, followed by reconstitution with CD45.1 bone

446 marrow (Figure 5D). We analyzed *Timd4*$^{+}$ and *Cx3cr1*$^{+}$ thymic macrophages
447 separately after 6 weeks because we suspected they might have different
448 origins. As Cx3cr1 protein expression was low on thymic macrophages
449 (Figure 5B), we defined the *Cx3cr1*$^{+}$*Timd4*$^{-}$ population as TIM4^{-}. The donor-
450 derived monocytes in the blood were, on average, 57%, but less than 2% of
451 TIM4^{+} thymic macrophages were CD45.1^{+} (Figure 5E and F), suggesting very
452 limited contribution of adult circulating monocytes to the TIM4^{+} macrophage
453 pool. The percentage of HSC-derived TIM4^{-} macrophages (on average 23%)
454 was intermediate between the monocytes and TIM4^{+} macrophages, pointing
455 out that a sizeable part of TIM4^{-} cells was derived from adult HSCs.
456 We also transplanted E15.5 embryonic thymuses from SpiC^{GFP+} CD45.2
457 under the kidney capsule of adult CD45.1 mice and analyzed them six weeks
458 later (Figure 5G). By that time, >99% of thymocytes in the transplanted
459 thymus were derived from CD45.1^{+} host HSCs, indicating successful
460 replacement by HSC-derived progenitors (Figure 5 – figure supplement 1).
461 TIM4^{-} thymic macrophages were derived entirely from host HSCs, just like
462 thymocytes. In contrast, most TIM4^{+} cells (on average 70%) were donor-
463 derived (Figure 5H and I). Moreover, only CD45.2^{+} TIM4^{+} macrophages
464 expressed SpiC^{GFP} (Figure 5 – figure supplement 2). As expected, thymic
465 macrophages in the endogenous thymus were all CD45.1^{+}. The results from
466 our transplantation experiments show that the progenitors of most TIM4^{+}
467 thymic macrophages are of embryonic origin, while TIM4^{-} cells are derived
468 from adult monocytes. Altogether our results suggest that the two populations
469 of thymic macrophages have different origins. TIM4^{+} cells are derived from
470 embryonic precursors and can survive long-term without much contribution

from adult HSC and monocytes. In contrast, TIM4^{-} thymic macrophages rely mostly on adult HSCs for their generation and replacement.

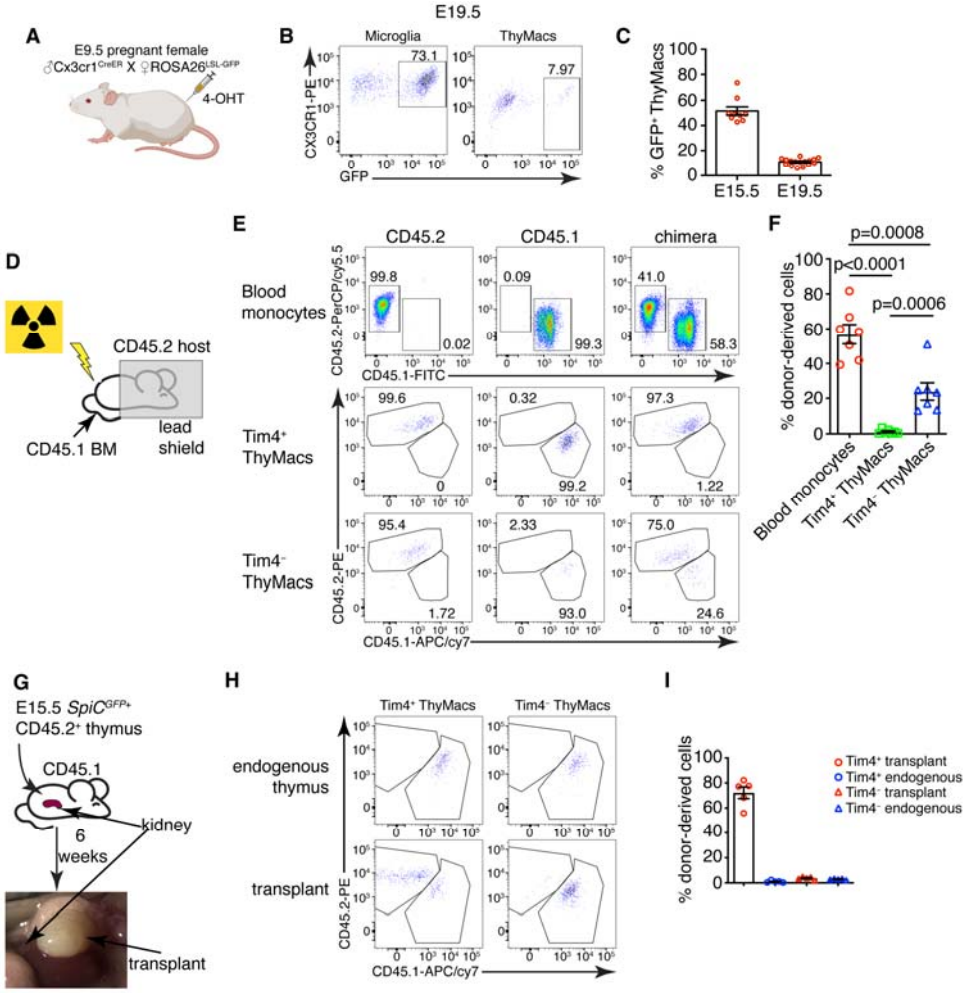

Figure 5. Yolk sac (YS), non-YS-derived embryonic progenitors, and adult hematopoietic stem cells sequentially contribute to the thymic macrophage pool. A Scheme of the YS-progenitor labeling experiments. E9.5 pregnant *ROSA26$^{LSL\text{-}GFP}$* mice mated with *Cx3cr1^{CreER}* males were injected with 4-hydroxytamoxifen (4-OHT) and sacrificed at E15.5 or E19.5. **B** Representative flow cytometry plots of the *Cx3cr1^{GFP}* expression in microglia (CD45^{+}CD11b^{+} cells in the brain) and ThyMacs of the pups at E19.5. **C** Frequencies of GFP^{+} ThyMacs at E15.5 and E19.5 adjusted to the degree of

labeling of microglia. **D** Scheme of the shield chimera experiments. Congenic CD45.2 mice were lethally irradiated with their upper body protected by a 5 cm thick lead shield and then injected with CD45.1^{+} bone marrow. **E** Representative flow cytometric analysis of CD115^{+}CD11b^{+} blood monocytes, TIM4^{+} and TIM4^{-} thymic macrophages for donor-derived (CD45.1^{+}) and host-derived (CD45.2^{+}) cells. Non-chimeric CD45.1 and CD45.2 samples serve as controls for the gating. **F** Frequencies of donor-derived blood monocytes, TIM4^{+} and TIM4^{-} ThyMacs. **G** Scheme of the thymus transplantation experiments. Embryonic thymuses from E15.5 SpiC^{GFP+} CD45.2^{+} mice were transplanted under the kidney capsule of CD45.1^{+} mice and analyzed six weeks later. **H** Representative flow cytometry plots of donor (CD45.2^{+}) vs. host (CD45.1^{+}) derived TIM4^{+} and TIM4^{-} ThyMacs in the transplanted thymus. The host thymus (endogenous thymus) serves as a negative control. I Frequencies of CD45.2^{+} (donor-derived) cells among TIM4^{+} and TIM4^{-} ThyMacs in the transplanted and endogenous thymuses of the mice. Data in **C**, **F**, and **I** are mean±SEM with two litters, seven, and five mice per group, respectively. The numbers in the flow cytometry plots are the percent of cells in the respective gates. Each symbol in the graphs is an individual mouse or embryo.

Thymic macrophages can proliferate in situ

TIM4^{+} macrophages can persist for many weeks in the thymus without constant replacement from blood monocytes, suggesting they can divide in situ. Staining for the proliferation marker Ki67 revealed that ~4% of all thymic macrophages expressed this marker compared to an isotype control (Figure

6A and B). To prove that thymic macrophages are proliferative, we tested the incorporation of the nucleotide analog 5-Ethynyl-2'-deoxyuridine (EdU). Short-term EdU labeling experiments unexpectedly revealed that thymic macrophages become EdU^+ with faster kinetics than thymocytes (Figure 6C). The most likely explanation for this puzzling result is that some of the thymic macrophages have engulfed apoptotic thymocytes that have recently divided and incorporated EdU. Thus, EdU could have accumulated in these macrophages through phagocytosis, not cell division. To circumvent this caveat, we designed a pulse-chase experiment (Figure 6D). Mice were injected daily with EdU for 21 days so that all cells that proliferated in that period would incorporate the label. Most thymocytes and thymic macrophages became EdU^+ at d. 21 (Figure 6E). After 21 more days of "chase period", only ~0.2% of thymocytes had retained the EdU label, consistent with the existence of a tiny population of long-term resident thymocytes consisting mainly of regulatory T cells and NKT cells[54] (Figure 6E and F). However, ~5% of the thymic macrophages were EdU^+, suggesting they divided during the labeling period. We also sorted thymic macrophages and subjected them to cell cycle analysis. Although almost all thymic macrophages were in G0/G1 phase, a small population of ~3% was in the G2/M phase of the cell cycle (Figure 6G and H). Surprisingly, most *Mki67*$^+$ thymic macrophages belonged to the *Cx3cr1*$^+$ subset, and only a few of the *Timd4*$^+$ cells were positive (Figure 6I). Collectively, four independent approaches documented that a small proportion (3-5%) of thymic macrophages are actively dividing under homeostatic conditions within the

thymus. The majority of the dividing cells were from the adult HSC-derived *Cx3cr1*$^{+}$ subset. *Timd4*$^{+}$ macrophages were primarily quiescent.

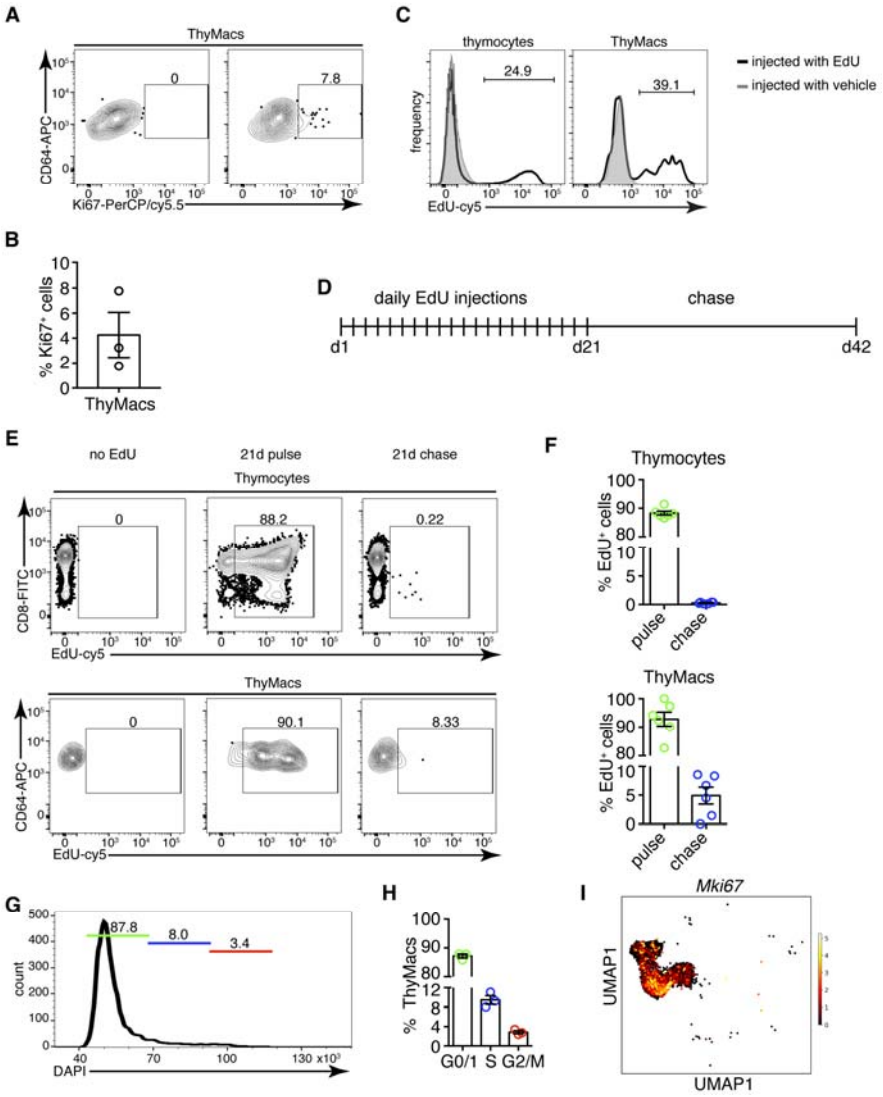

Figure 6. Thymic macrophages exhibit a low degree of proliferation. **A** Example flow cytometry plots of Ki67 staining of thymic macrophages (ThyMacs). **B** Frequency of Ki67^{+} thymic macrophages. **C** Example flow cytometry plots of the EdU accumulation in thymocytes and thymic macrophages 2 hours after 1 mg EdU i.p. or vehicle injection. The numbers inside flow plots are the percentage of EdU^{+} cells from mice injected with EdU. Data are representative of three independent experiments. **D** Scheme of

EdU pulse/chase experiment: mice were injected daily with 1 mg EdU i.p for 21 days and rested for 21 more days. **E** Example flow cytometry plots of EdU staining of thymocytes (upper row) and ThyMacs (lower row). **F** Frequencies of EdU$^+$ cells among thymocytes (top graph) and ThyMacs (bottom graph). **G** Example flow cytometry plot of cell cycle analysis of FACS sorted ThyMacs. **H** Frequencies of ThyMacs in different stages of the cell cycle. **I** UMAP plot of *Mki67* expression in *Mafb*-positive clusters from the scRNA-Seq data described in Figure 4. The numbers in the flow cytometry plots are the percent of cells in the respective gates. Data are mean±SEM from three mice (**B** and **H**) or 6-7 individual mice (**F**). Each dot is an individual mouse.

***Cx3cr1*$^+$ cells give rise to *Timd4*$^+$ cells during embryonic development**

To determine if the two populations of thymic macrophages are related, we first analyzed the kinetics of their appearance during embryonic development. At the earliest time point (E14.5), all thymic macrophages were *Cx3cr1*$^+$, and only ~20% were also TIM4$^+$ (Figure 7A and B). The proportion of TIM4$^+$ cells increased at E17.5, and TIM4$^+$*Cx3cr1*$^-$ cells started to appear. In the neonatal period, almost all macrophages were TIM4$^+$, and very few remained TIM4$^-$. The proportion of TIM4$^-$ cells increased in 6 weeks old mice, but TIM4$^+$ macrophages remained the dominant population. These kinetics (Figure 7C) are consistent with *Timd4*$^+$ macrophages developing from *Cx3cr1*$^+$ cells before birth. Another plausible scenario is that distinct progenitors give rise to different thymic macrophage populations (e.g., YS-progenitors give rise to *Cx3cr1*$^+$*Timd4*$^-$ and HSC-derived progenitors develop into *Timd4*$^+$ macrophages). To test the latter hypothesis, we revisited the fate mapping of

YS progenitors (Figure 5A). Although a larger part (~60% at E15.5) of fate-mapped cells were *Cx3cr1*$^{+}$TIM4^{-} cells (Figure 7D), a substantial proportion (~40% at E15.5) of fate-mapped TIM4^{+} macrophages could clearly be identified at both E15.5 and E19.5, suggesting that YS progenitors can give rise to both *Cx3cr1*$^{+}$ and *Timd4*$^{+}$ cells. Thus, the simplest explanation for our findings is that *Timd4*$^{+}$ cells develop from *Cx3cr1*$^{+}$ cells during embryonic development. This transition is complete in the first week after birth as there were essentially no *Cx3cr1*$^{+}$TIM4^{-} thymic macrophages remaining at d.7 (Figure 7A and B). To formally demonstrate that *Cx3cr1*$^{+}$ macrophages can give rise to *Timd4*$^{+}$ cells during embryonic development, we injected 4-OHT in E15.5 pregnant females carrying Cx3cr1^{CreER} X ROSA26$^{LSL\text{-}GFP}$ fetuses (Fig. 7E). At this time almost all thymic macrophages are *Cx3cr1*$^{+}$ (Fig. 7A). Just before birth, at E19.5, we could identify a sizeable population of TIM4^{+}CX3CR1^{-} among fate-mapped cells, suggesting that they originate from *Cx3cr1*$^{+}$ progenitors (Fig. 7F and G).

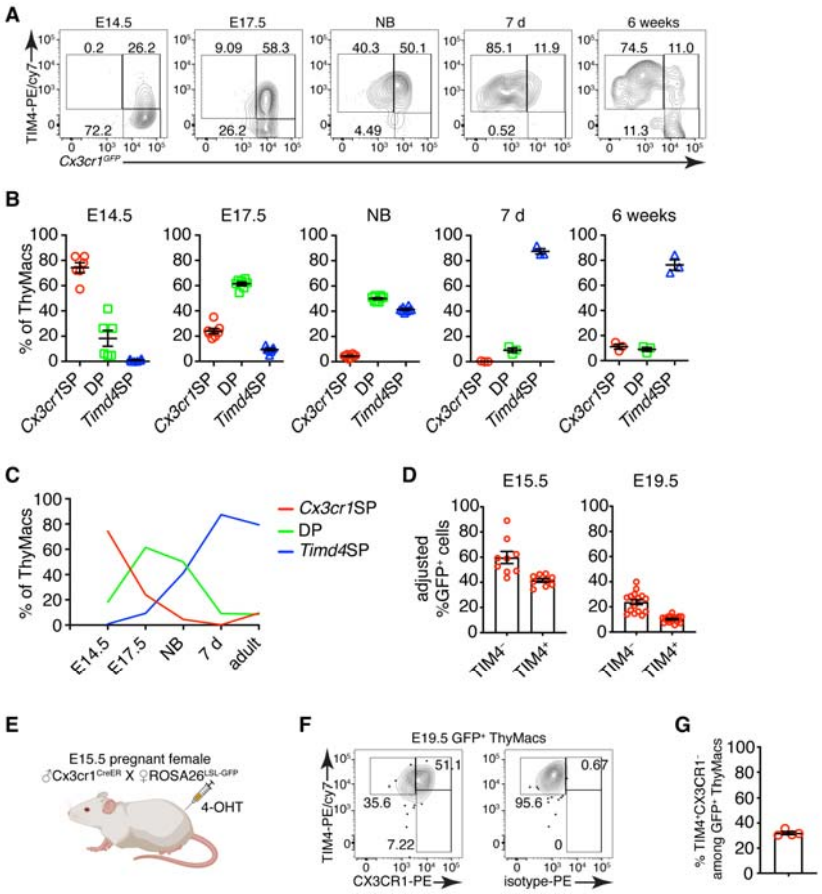

Figure 7. *Timd4*$^{+}$ thymic macrophages are derived from *Cx3cr1*$^{+}$ cells during embryonic development. A Example flow cytometry plots for the expression of *Cx3cr1*^{GFP} and TIM4 on thymic macrophages at different times during embryonic development (E14.5, E17.5), immediately after birth, at 7 days, and 6 weeks of age. **B** Frequencies of *Timd4*$^{+}$*Cx3cr1*$^{-}$ (*Timd4* single-positive or *Timd4*SP), *Timd4*$^{+}$*Cx3cr1*$^{+}$(double-positive or DP), and *Cx3cr1*$^{+}$*Timd4*$^{-}$ (*Cx3cr1* single-positive or *Cx3cr1*SP) thymic macrophages at the indicated time points. **C** Kinetics of the changes in different subpopulations of thymic macrophages from E14.5 to 6 weeks. **D** Frequencies at E15.5 and E19.5 of GFP-labeled cells among TIM4^{+} or TIM4^{-} cells in *Cx3cr1*^{CreER} X *ROSA26*$^{LSL\text{-}GFP}$ embryos treated with 4-OHT at E9.5. **E** Scheme of the fate-mapping experiments showing the relationship between *Cx3cr1*$^{+}$ and *Timd4*$^{+}$

thymic macrophages during embryonic development. E15.5 pregnant *ROSA26*$^{LSL\text{-}GFP}$ mice mated with *Cx3cr1*^{CreER} males were injected with 4-hydroxytamoxifen (4-OHT) and sacrificed at E19.5. **F** Representative flow cytometry staining for TIM4 and CX3CR1 in fate-mapped GFP^{+} thymic macrophages at E19.5. The panel to the right is the isotype control for CX3CR1-PE staining. **G** Frequencies of TIM4^{+}CX3CR1^{-} cells among fate-mapped GFP^{+} macrophages. Data are from at least two independent experiments for each panel. Each symbol is an individual mouse or embryo.

***Cx3cr1*$^{+}$ *thymic macrophages slowly accumulate with age at the expense of Timd4*$^{+}$ cells**

To understand the dynamics of the two resident thymic macrophage populations with age, we induced recombination in *Cx3cr1*^{CreER} X *ROSA26*$^{LSL\text{-}GFP}$ mice during the neonatal period (Figure 8A) or at 6 weeks of age (Figure 8C) and compared the proportion of GFP^{+} cells 3 and 42 days after labeling. The extent of labeling of TIM4^{+} thymic macrophages did not change within these 6 weeks, no matter whether the mice were treated with Tamoxifen in the first week after birth or at 6 weeks (Figure 8B and D), suggesting an absence of a significant influx from unlabeled cells (e.g., monocytes). In contrast, the proportion of labeled TIM4^{-} thymic macrophages decreased significantly 6 weeks after Tamoxifen injection in neonatal and adult mice, suggesting that this population was diluted by unlabeled cells. To further substantiate these findings, we examined older WT mice and found out that the proportions of TIM4^{-} thymic macrophages increased with age, and in mice >8 months old, they accounted for ~70% of all macrophages in the organ

(Figure 8E). As these changes in the proportions of the thymic macrophage subpopulations occurred at the background of thymic involution, we wanted to know if the accumulation of TIM4^{-} cells was only relative or also in absolute cell numbers. In contrast to TIM4^{+} thymic macrophages that reached peak numbers at an early age and then declined significantly, TIM4^{-} cells tended to increase their numbers in older mice (Figure 8F). Thus, we conclude that, after birth, the numbers of TIM4^{+} macrophages follow the kinetics of the thymus size – increase in young and decrease in old mice, and they are not replaced by other cells. In contrast, since the first week of life, *Cx3cr1*$^{+}$ cells are recruited to the thymus, accumulate with age, and in old mice, form the predominant phagocytic population in the organ.

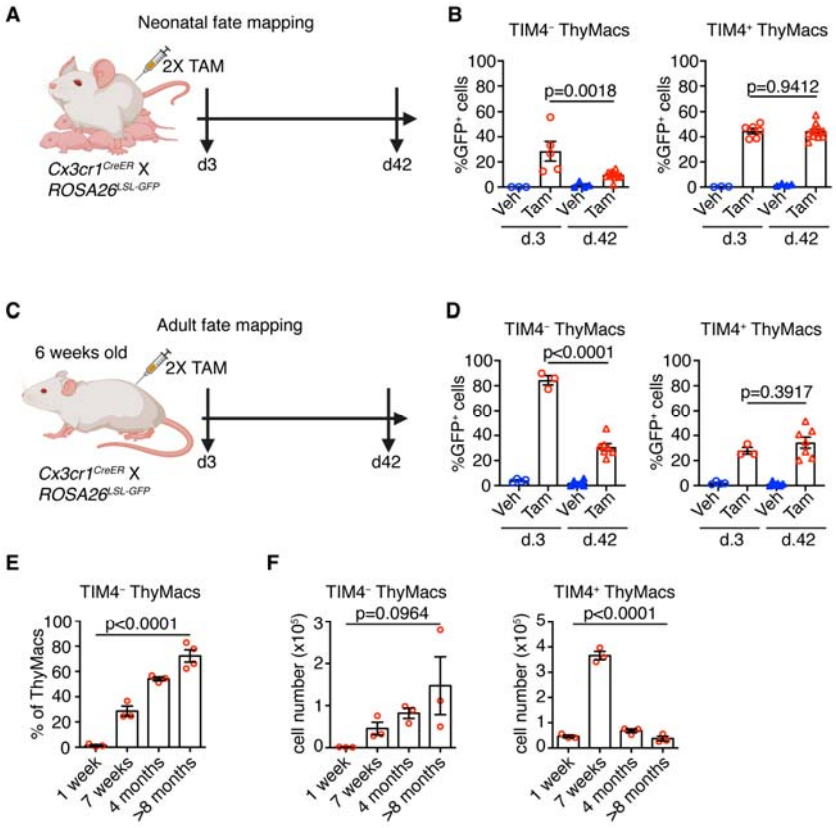

Figure 8. *Timd4*$^{+}$ thymic macrophages are progressively lost, while *Cx3cr1*$^{+}$ cells slowly accumulate with age. A Scheme of the neonatal fate

mapping: A nursing dam was injected twice with Tamoxifen (Tam) or vehicle (Veh) in the first week after giving birth to *Cx3cr1*^{CreER} X *ROSA26*$^{LSL\text{-}GFP}$ pups. The mice were sacrificed three or 42 days after the last injection, and the degree of labeling of TIM4^{+} and TIM4^{-} thymic macrophages was examined by flow cytometry. **B** Frequencies of GFP^{+} TIM4^{+} or TIM4^{-} thymic macrophages from neonatally fate-mapped mice after 3 and 42 days. Vehicle-injected nursing dam litters (Veh) served as a control for non-specific labeling. **C** Scheme of the adult fate mapping: Six weeks old *Cx3cr1*^{CreER} X *ROSA26*$^{LSL\text{-}GFP}$ mice were injected twice with Tamoxifen (Tam) or vehicle (Veh). The mice were sacrificed three or 42 days after the last injection, and the degree of labeling of TIM4^{+} and TIM4^{-} thymic macrophages was examined by flow cytometry. **D** Frequencies of GFP^{+} TIM4^{+} or TIM4^{-} thymic macrophages from adult fate-mapped mice after 3 and 42 days. **E** Frequencies of TIM4^{-} thymic macrophages at different ages. **F** Changes in the numbers of TIM4^{-} and TIM4^{+} thymic macrophages with age. The data are mean±SEM from 2 independent experiments (**B**) or at least 3 individual mice per time point (**D**, **E**, and **F**). Each symbol is an individual mouse. Statistical significance in the difference between Tamoxifen-treated samples at different time points was determined with unpaired Student's t-test (**B** and **D**). One-way ANOVA was used to assess the significance of the change in TIM4^{+} and TIM4^{-} ThyMacs percentages and numbers with age (**E** and **F**).

Discussion

Here, we have described the phenotype, transcriptional profile, localization, diversity, ontogeny, and maintenance of macrophages in the thymus. These

cells express the typical macrophage markers CD64, MerTK, and F4/80 and are transcriptionally most similar to splenic red pulp macrophages and liver Kupffer cells. However, they have a unique expression profile dominated by genes involved in antigen presentation and lysosomal degradation. We found that thymic macrophages consist of two populations with distinct localization. *Timd4*$^{+}$ macrophages occupied the cortex, while *Cx3cr1*$^{+}$ cells were located in the medulla and the cortico-medullary junction. While YS-derived macrophages dominated the early stages of thymus development, they were quickly replaced by non-YS embryonic progenitors that gave rise to the *Timd4*$^{+}$ thymic macrophages that persisted into adulthood and formed the main macrophage population in young mice. *Cx3cr1*$^{+}$ macrophages slowly accumulated after birth and became the most abundant population in old mice.

Altogether our data depict thymic macrophages as typical tissue-resident macrophages originating from multiple hematopoietic waves, surviving long-term, and expressing the core macrophage-specific genes. They are most similar transcriptionally to splenic red pulp macrophages and Kupffer cells, which is not surprising considering that they all specialize in efferocytosis and have efficient lysosomal degradation machinery. These three populations also shared expression of the transcription factor *Spic* that is induced by heme released following red blood cells phagocytosis[52]. However, the thymus is not known as a place for erythrocyte degradation. Thus, the mechanism for *Spic* up-regulation in thymic macrophages is unclear.

The unique features of thymic macrophages include high expression of genes involved in the IFN-I pathway, antigen presentation, and lysosomal

degradation. The up-regulation of IFN-I-stimulated genes such as *Stat1*, *Stat2*, *Irf7*, and *Irf8* can be explained by the constitutive secretion of IFN-I by thymic epithelial cells[55,56]. The purpose of IFN-I expression in the thymus in the absence of a viral infection is unclear. Still, one possibility is that it mediates negative selection to IFN-dependent genes as part of central tolerance.

Thymic macrophages highly express molecules involved in antigen presentation, including MHC1 and MHC2, although the latter is expressed at lower levels than in cDCs, and are functionally competent to induce T cell activation. Thus, they have the potential to present antigens for both negative selection and agonist selection. These two activities have traditionally been assigned solely to cDCs[57]. However, recent evidence suggests that negative selection is most efficient when the cell that presents the antigen to auto-reactive thymocytes is also the one that phagocytoses it[58]. So, macrophages' participation in thymocyte selection needs to be re-evaluated.

The extraordinary ability of thymic macrophages to engulf and degrade apoptotic thymocytes has been appreciated for a long time[31], and our RNA-Seq data provides additional supporting evidence for this function by highlighting the up-regulation of pathways involved in lysosomal degradation. An interesting topic for future research would be understanding how the metabolites derived from apoptotic cells are returned to the microenvironment to support the proliferation of immature thymocytes. A *SoLute Carrier* (*Slc*) genes-based program has been described in vitro[59], but its relevance to tissue-resident macrophages remains to be determined. Altogether, our study demonstrates that thymic macrophages are a unique subset of tissue-resident

macrophages and support the idea that resident macrophage phenotype is determined by the combination of ontogeny, microenvironment, and other factors[60].

Together with the study by Tacke et al., our work builds the following model for thymic macrophage origin[37]: Thymic macrophages develop in three distinct waves: YS-derived progenitors dominate the early stages of thymus development but are replaced before birth by a second wave of YS-independent embryonic progenitors that forms the bulk of thymic macrophages after birth and can self-maintain into adulthood. With age, there is a slow and steady influx of *Timd4*$^{-}$*Cx3cr1*$^{+}$ macrophage precursors that occupy the medulla and cortico-medullary junction, becoming the major phagocytic population in the thymus of older mice (>8 months). The second wave of YS-independent macrophages is most likely the progeny of embryonic HSCs based on *Flt3*^{Cre} fate mapping that showed that >80% of thymic macrophages in adult mice are descendants of HSCs[37]. Whether HSC-independent fetal liver monocytes contribute to thymic macrophages and to what extent awaits the creation of models that can specifically target this population of progenitors. Recruitment of circulating monocytes to the resident macrophage pool in the thymus has been ruled out previously by parabiosis and *Ccr2*$^{-/-}$ mice[37]. Our shield chimera experiments have arrived at similar conclusions. However, the relatively short duration of these experiments and their focus on the bulk thymic macrophages have prevented the recognition of the gradual accumulation of *Timd4*$^{-}$ macrophages. Once we zoomed in on this minor cell population in young mice, the fate mapping clearly showed an influx of unlabeled progenitors. Whether the progenitors of *Timd4*$^{-}$ macrophages

are monocytes remains to be formally demonstrated. However, monocytes have been singled out as the source of all macrophage populations exhibiting replacement in adults examined to date[12,19,22,24,25,30]. An alternative possibility involves thymocyte progenitors that, under certain circumstances, have been shown to differentiate into macrophages and granulocytes in the thymus[42,43]. However, if this occurs in unmanipulated mice at a steady state remains unclear.

The spatial segregation of the two macrophage populations in the thymus implies that they might have distinct functions. *Timd4*$^+$ cells are restricted to the cortex and are particularly abundant in the deeper cortex, close to the medulla. Both positive and negative selection of thymocytes occur there, so we speculate that *Timd4*$^+$ macrophages might be specialized in efferocytosis of CD4$^+$CD8$^+$ (double-positive) thymocytes that cannot interact with cortical thymic epithelial cells and die by neglect or are auto-reactive and undergo clonal deletion in the cortex[61]. On the other hand, *Cx3cr1*$^+$ macrophages accumulate in the medulla – the thymic region specialized in negative selection to tissue-restricted antigens (TRA). They might contribute to the process in several ways: 1) by carrying TRAs from blood and peripheral organs. A similar process has been described for cDC2 (SIRPα^+ DCs)[62]. In fact, *Cx3cr1*$^+$ thymic macrophages could have contributed to this role because they were not distinguished from cDC2 in this study. 2) By capturing TRAs from *Aire*$^+$ medullary thymic epithelial cells and presenting them to auto-reactive thymocytes as shown for DCs[63-65]. 3) By phagocytosing apoptotic TRA-specific medullary thymocytes, a process we have observed before[58].

The exact involvement of thymic macrophages in the selection events in the thymus remains to be determined.

The accumulation of the *Cx3cr1*$^{+}$ cells in older mice has clear implications for thymus aging. One key feature of thymus involution is the accumulation of extracellular matrix produced by fibroblasts and the emergence of white adipocytes[66]. The *Cx3cr1*$^{+}$ subset is the predominant producer of the growth factor PDGFα that is required for the maintenance of adipocyte stem cells and can stimulate tissue fibrosis[67,68]. The gradual accumulation of *Cx3cr1*$^{+}$ macrophages could increase the availability PDGFα in the aging thymus stimulating extracellular matrix production and differentiation of precursors into adipocytes. This model predicts that limiting the influx of *Cx3cr1*$^{+}$ macrophage precursors could delay thymus involution.

Recent work described a novel phagocytic and antigen-presenting cell type in the thymus called monocyte-derived DCs[65]. The phenotype of these cells overlaps with the CD64^{+}F4/80^{lo}CD11b^{+} cells in our study. However, we favor the classification of these cells as monocytes based on their expression of *Mafb*, CD64, and Ly6C (Figure 4D) and lack of expression of the defining DC transcription factor *Zbtb46* (Figure 4B)[69]. As monocytes can differentiate into cDC2, particularly in the context of inflammation[70], the precise identity and the relationship of this population to thymic cDC2 remain to be established.

In the past several years, scRNA-Seq has come to the forefront of biologists' efforts to disentangle the cellular diversity of tissues. Several comprehensive studies have included samples from mouse or human thymus[71-73]. However, too few thymic macrophages were sampled in

these studies to give meaningful clustering results. Efforts specifically targeting the thymus have provided considerably more information[74,75], but macrophage diversity was still not recognized. Characterization of rare populations such as thymic macrophages (~0.1% of all cells in the thymus) requires optimized enzymatic digestion procedures and enrichment strategies, as has already been demonstrated for thymic epithelial cells[76,77]. Our scRNA-Seq dataset provides a rich resource for the unbiased characterization of myeloid cells in the thymus and will greatly aid in the understanding of the myeloid landscape of the thymus.

In summary, our work comprehensively characterizes macrophages in the thymus and paves the way for the exploration of their functions.

Materials and methods

Mice

C57BL/6Narl (CD45.2) mice were purchased from the National Laboratory Animal Center, Taipei, Taiwan. MAFIA (MAcrophage Fas-Induced Apoptosis) [78], *Cx3cr1*^{GFP} [79], *Spic*^{GFP} [52], *Cx3cr1*^{CreER} [53], and *B6.SJL-Ptprca Pepcb/BoyJ* (CD45.1) mice were purchased from the Jackson Laboratories. *Cd11c*^{YFP} [80] and *Lyz2*^{GFP} [81] mice have been described. Mice ubiquitously expressing GFP from the *ROSA26* locus were generated by breeding *Pdgfra*^{Cre} [82] and *ROSA26*$^{LSL\text{-}ZsGreen}$ (also known as *ROSA26*$^{LSL\text{-}GFP}$ or Ai6) mice[83] (both from the Jackson Laboratories). A mouse from this cross was identified, in which the STOP cassette was deleted in the germline. It was designated *ROSA26*^{GFP} and subsequently bred to C57BL/6 mice. All mice were used at 4-10 weeks of age unless otherwise specified. Mice were bred

807 and maintained under specific pathogen-free conditions at the animal facility
808 of National Yang-Ming University. All experimental procedures were approved
809 by the Institutional Animal Care and Use Committee (IACUC) of National
810 Yang Ming Chiao Tung University.
811
812 **Treatment with 5-Ethynyl-2'-deoxyuridine (EdU)**
813 Mice were i.p. injected with 1 mg EdU (Carbosynth) dissolved in PBS daily
814 for 21 days and then rested for 21 more days. Cells from the thymus were
815 harvested on day 21 or 42. In some experiments, the mice were sacrificed 2
816 hours after the first EdU injection.
817
818 **Shield chimera generation**
819 WT (CD45.2) mice were anesthetized by i.p. injection of 120 µg/g body
820 weight Ketamine hydrochloride (Toronto Research Chemicals) and 12 µg/g
821 body weight Xylazine hydrochloride (Sigma). Anesthetized mice were taped
822 to a 5 cm thick lead block so that the lead block covered the head and the
823 chest down to the bottom of the rib cage. Then, they were irradiated with a
824 lethal dose (1000 rad) from a ^{137}Cs source (Minishot II, AXR) so that only their
825 abdomen and hind legs were exposed. After recovery from anesthesia, the
826 mice were transfused i.v. with 10^7 bone marrow cells from a congenic
827 (CD45.1) donor. Then, they were given Trimerin (0.5 mg/mL Sulfadiazine +
828 0.1 mg/mL Trimethoprim, China Chemical and Pharmaceutical Co., Tainan,
829 Taiwan) in the drinking water for the first two weeks after the irradiation and
830 analyzed after six weeks.
831

Cell isolation from thymus, blood, and peritoneal cavity

Thymocytes were obtained by mechanical disruption of the thymus with a syringe plunger. For myeloid cell isolation, mouse thymuses were cut into small pieces and digested with 0.2 mg/mL DNase I (Roche) and 0.2 mg/mL collagenase P (Roche) in complete DMEM for 20 min at 37˚C with frequent agitation. In some experiments, thymic myeloid cells were enriched by 57% Percoll PLUS (GE Healthcare) discontinuous gradient centrifugation at 4˚C, 1800 rpm, for 20 min without brake. Cells at the interface were collected and washed with PBS to remove residual silica particles. Then the cells were resuspended in PBS with 0.5% BSA (HM Biological), filtered through a 70 µm filter, and kept on ice.

Blood was isolated by cardiac puncture of sacrificed mice and immediately diluted with PBS. After centrifugation, the cell suspensions were treated with ammonium chloride-potassium lysis buffer for 3 min on ice once or twice. Peritoneal cavity cells were obtained by lavage with 5 mL PBS + 2 mM EDTA (Merck). Following gentle massage, the cavity was opened with an abdominal incision, and lavage fluid was collected.

Flow cytometry

Single-cell suspensions (0.5 – 2X10^6 cells) from thymus, blood, or peritoneal cavity were blocked with supernatant from 2.4G2 hybridoma (a kind gift by Dr. Fang Liao, Academia Sinica, Taipei, Taiwan) and stained with fluorochrome- or biotin-labeled antibodies for 20 min on ice in PBS + 0.5% BSA + 2 mM EDTA + 0.1% NaN_3 (FACS buffer). The following antibodies

were used: CD11b (clone M1/70), MHC2 (M5/114.15.2), CD11c (N418), F4/80 (BM8), CD115 (AFS98), SIRPα (P84), CD45 (30-F11), NK1.1 (PK136), TIM4 (RMT4-54), Gr-1 (RB6-8C5), CD64 (X54-5/7.1), Siglec H (551), Ly6C (HK1.4), CD3ε (145-2C11), CD8α (53-6.7), CD19 (6D5), B220 (RA3-6B2), CD4 (GK1.5), CD51 (RMV-7), CD45.1 (A20), CD45.2 (104), CX3CR1 (SA011F11), and EpCAM (G8.8) from BioLegend; Axl (MAXL8DS), MerTK (DS5MMER), and Ki67 (SolA15) were from eBioscience; Siglec F (E50-2440), CD90.2 (30-H12), and CD11c (HL3) were from BD Biosciences. Cells were washed, and if necessary, incubated for 20 more min with fluorochrome-labeled Streptavidin: Streptavidin-AF647 (Jackson Immunoresearch) or Streptavidin-APC/cy7, Streptavidin-BV421, Streptavidin-BV605 (BioLegend). After the last wash, the cells were resuspended in FACS buffer containing DAPI (BioLegend), Propidium Iodide (Sigma), or DRAQ7 (BioLegend) and analyzed immediately on an LSR Fortessa flow cytometer running Diva 8 software (BD Biosciences). Typically, 500,000 cells were collected from thymus samples. Data were analyzed using FlowJo software (TreeStar).

For intracellular staining, after surface antibody staining, the cells were labeled with Zombie Aqua (BioLegend) for 30 min in ice. Then, the cells were fixed with 2% paraformaldehyde (Electron Microscope Sciences) in PBS for 20 min on ice, permeabilized with either 0.5% Triton-X 100 (Sigma) for 20 min on ice, or with Foxp3 staining kit (eBioscience) according to the protocol provided by the manufacturer, and stained with antibodies for intracellular markers for 40-60 min on ice.

For cell cycle analysis, 1-5x10^5 sorted thymic macrophages were fixed with 70% ethanol for 2 h on ice. The cells were spun down at 1800 rpm for 20 min at 4˚C, washed with PBS, and stained with 1 μg/ml DAPI (BioLegend) for 30 min at room temperature in the dark.

For EdU staining, after surface marker and Zombie Aqua staining, cells were fixed with 2% paraformaldehyde in PBS for 20 min on ice and permeabilized with 0.5% Triton X-100 in PBS at room temperature for 20 min. EdU was detected by adding an equal volume of 2X Click reaction buffer consisting of 200 mM Tris, 200 mM ascorbic acid (Acros), 8 mM $CuSO_4$ (Acros), 8 μM Cy5-azide (Lumiprobe) to the permeabilized cells resuspended in 0.5% Triton X-100 in PBS and incubation at room temperature for 30 min. Cells were washed twice with 0.5% Triton X-100 in PBS and analyzed on a flow cytometer.

Cell sorting

The sorting of thymic macrophages was done following the IMMGEN guidelines. Briefly, the thymuses of 3 male C57BL/6Narl mice were harvested in ice-cold staining buffer containing phenol red-free DMEM (Gibco) with 10 mM HEPES (Sigma), 0.1% NaN_3, and 2% FBS (Gibco). Single-cell suspensions were prepared as described in the Flow cytometry section. Percoll PLUS was used to enrich mononuclear cells. The cells were resuspended at 10^8/mL in staining buffer and labeled with appropriate antibodies for 15 min in ice. To sort thymic macrophages, the cells were first labeled with biotinylated antibodies to lineage markers (Lin) – CD3, CD8, Gr1,

907 B220. After washing, the cells were stained with antibodies to CD11b, F4/80,
908 CD45, CD64, and Streptavidin-APC/cy7 for 15 min in ice. For sorting thymus
909 XCR1^{+} and SIRPα^{+} cDCs, antibodies to XCR1, SIRPα, CD11c, MHC2, CD64,
910 and F4/80 were used. For sorting peritoneal cavity macrophages, antibodies
911 to ICAM2 and F4/80 were used. Immediately before sorting, the dead cells
912 were excluded with DRAQ7 or PI. For RNA Sequencing experiments, the
913 cells were double-sorted on FACS Melody, or Aria cell sorters (BD
914 Biosciences) and 1000 cells were directly deposited in TCL buffer (Qiagen),
915 frozen in dry ice and sent to IMMGEN for RNA sequencing. Four biological
916 replicates were prepared. For cytospin and cell cycle analysis, 1-5x10^{5} cells
917 sorted on FACS Melody were collected in staining buffer.
918
919 **Cytospin**
920 Sorted cells were mounted on Superfrost PLUS slides (Thermo Scientific)
921 using a Cytospin centrifuge (Cytospin 3, Shandon) for 5 min at 500 rpm. Cells
922 were fixed with 2% paraformaldehyde for 10 min at room temperature and
923 stained with the Hemacolor Rapid Staining Kit (Merck Millipore). Images were
924 collected on BX61 upright microscope (Olympus) using 100X objective with
925 immersion oil and captured with a CCD camera. Images were then analyzed
926 and processed with ImageJ (NIH) and Adobe Photoshop 5.5 (Adobe).
927
928 **In vitro phagocytosis assay**
929 10^{7} Thymocytes were cultured in cDMEM in the presence of 1 μM of
930 dexamethasone (Sigma) in a 3.5-cm culture dish at 37℃ in 5% CO_2 incubator
931 for 8 hours. Apoptosis levels were assessed by PI (Biolegend) and Annexin V-

FITC (Biolegend) staining. Typically, more than 80% of cells were Annexin V^+. The dexamethasone-treated thymocytes were stained with 1 µg/mL pHrodo Red, SE (ThermoFisher) in PBS for 30 min at room temperature. The cells were washed two times with cDMEM and resuspended at $2x10^6$ cells/mL. $4x10^4$ sorted peritoneal and thymic macrophages were stained with 5 µM eFluor 450 (Thermo Fisher) in PBS for 10 min at 37℃, washed two times with cDMEM and cultured in 96-well flat-bottom culture plate (Nunc) in 100 µL cDMEM at 37℃ in 5% CO_2 incubator. After 3 hours of attachment, the non-adherent cells were removed, and 200 µL ($4x10^5$) apoptotic thymocytes were added to the macrophages. The cells were incubated at 37℃ in 5% CO_2 incubator for 2 hours. Fluorescent images were captured with AxioObserver 7 (Carl Zeiss) wide-field microscope equipped with Plan Apochromat 40x NA=1.0 objective (Zeiss) and AxioCam 702 monochrome camera (Zeiss) controlled by Zen 2.3 Blue (Zeiss) software. Image analysis was performed with Imaris 8.0.2 (Bitplane). Phagocytosis was scored by investigators blinded to the samples' identities.

In vitro antigen presentation assay

$3x10^4$ sorted thymic $CD64^-MHCII^+CD11c^+$ dendritic cells, thymic, or peritoneal macrophages were cultured in 96-well round-bottom culture plate in 100 µL cDMEM at 37℃ in 5% CO_2 incubator for 3 hours to attach. Splenocytes from OT2 mice were stained with biotinylated antibodies to CD8a, CD11b, CD11c, B220, and MHCII (all from BioLegend), washed, and labeled with anti-biotin Microbeads (Miltenyi) plus CD44 microbeads (Miltenyi) in cRPMI. The cells were separated on MACS LS columns (Miltenyi)

according to the manufacturer's instructions. Enriched cells (naïve CD4 T cells) were stained with 10 µM CFSE (Sigma) for 5 min in PBS at 37℃ and cocultured with the sorted thymic MHCII^{+}CD11c^{+} dendritic cells, thymic, or peritoneal macrophages, in the presence or absence of 0.5 mg/mL OVA protein (Sigma) in cRPMI at 37℃ in 5% CO_2 incubator for 72 hours. The cells were collected and stained with antibodies to TCRβ and CD4 (from BioLegend) for flow cytometry analyses of CFSE dilution. The data were analyzed with FlowJo's Proliferation Modelling module (BD Biosciences).

RNA sequencing analysis

RNA sequencing was done at IMMGEN using Smart-seq2 protocol[84,85] on a NextSeq500 sequencer (Illumina). Following sequencing, raw reads were aligned with STAR to the mouse genome assembly mm10 and assigned to specific genes using the GENCODE vM12 annotation. Gene expression was normalized by DESeq2[86] and visualized by Morpheus (https://software.broadinstitute.org/morpheus). The principal component analysis was done by plotPCA() function of R package "DESeq2. Gene expression of mouse transcription factors[87] was visualized in MultiplotStudio of GenePattern[88]. GO enrichment was calculated and visualized in R by using clusterProfiler[89].

Timed pregnancies and embryonic thymus analysis

To set up timed pregnancies, each male mouse (*Cx3cr1*$^{CreER/CreER}$, *Cx3cr1*$^{GFP/GFP}$ or C57BL/6) and female mouse (*ROSA26*$^{LSL\text{-}GFP/LSL\text{-}GFP}$ or

C57BL/6) were housed together in the same cage for one night and separated on the next day, which we defined as embryonic day 0.5 (E0.5). Female mice were assumed to be pregnant if their weight gain was over 2 g at E8.5[90]. Thymuses from E14.5 and E17.5 embryos, neonatal, 1-weeks-old pups, and adult mice (older than 6-weeks-old) were harvested, mechanically dissociated with plastic sticks in 1.5-mL centrifuge tubes, and enzymatically digested with 0.2 mg/mL DNase I and 0.2 mg/mL collagenase P in complete DMEM for 20 min at 37˚C with frequent agitation. The cells were resuspended in PBS with 0.5% BSA, filtered through a 70 µm filter, kept on ice, and used flow cytometric analysis as described in the Flow Cytometry section.

Genetic fate mapping – E9.5, neonatal and adult

For genetic fate mapping, timed pregnancies of *Cx3cr1*$^{CreER/CreER}$ male and *ROSA26*$^{LSL\text{-}GFP/LSL\text{-}GFP}$ female mice were set up as described. To label the *Cx3cr1*$^{+}$ erythromyeloid progenitors derived from embryonic yolk sac[8], 4-hydroxytamoxifen (4-OHT from Sigma) was administered i.p. to pregnant females on E9.5 at a dose of 75 µg/g (body weight). To improve the survival of embryos and reduce the risk of abortions, Progesterone (Sigma) was co-injected at a dose of 37.5 µg/g (body weight)[91]. To label the *Cx3cr1*$^{+}$ thymic macrophages in *Cx3cr1*^{CreER} X *ROSA26*$^{LSL\text{-}GFP}$ neonates and adult mice, Tamoxifen (TAM from Sigma) was injected i.p. at a dose of 2 mg/mouse to lactating dams on postnatal day 3 and 4 (P3 and P4) or to adult mice for 2 consecutive days. Thymuses were harvested and analyzed 3 days or 6 weeks after the last injection by flow cytometry.

scRNA-Seq – sorting, library generation, and sequencing

scRNA-Seq was performed at the Genomics Center for Clinical and Biotechnological Applications of NCFB (NYCU, Taipei, Taiwan). Briefly, the thymuses of one female MAFIA and 2 male *Cd11c*^{YFP} mice were harvested and enzymatically digested as described previously. Mononuclear cells were enriched by 57% Percoll PLUS discontinuous centrifugation, washed to remove silica particles, and resuspended at 10^6/mL in PBS with 0.04% BSA. The cell suspensions were filtered through Falcon 35 µm strainer (Corning) and stained with viability dye (PI or DAPI) immediately before sorting. Cell sorting was performed on a FACS Melody sorter (BD Biosciences) running FACS Chorus (BD Biosciences) software in purity mode. $3X10^5$ GFP or YFP positive cells under the live/singlet gating were collected into 5 ml round bottom tubes pre-coated with 0.04% BSA in PBS. Sorted cells were washed and resuspended in 300 µL PBS with 0.04% BSA and then filtered again into 1.5-mL DNA LoBind tubes (Eppendorf) through a 35 µm strainer. The viability of the cells was evaluated by Countess II (Invitrogen) and Trypan Blue (ThermoFisher), and samples with cell viability rates higher than 85% were used for encapsulation and library preparation. Single-cell encapsulation and library preparation were performed using Single Cell 3' v3/v3.1 Gene Expression solution (10x Genomics). All the libraries were processed according to the manufacturer's instruction and sequenced on NovaSeq 6000 (Illumina) platform at the NHRI (Zhubei, Taiwan). Post-processing and quality control were performed by the NYCU Genome Center using the CellRanger package (v. 3.0.2, 10x Genomics). Reads were aligned to mm10 reference assembly. Primary assessment with CellRanger reported 9,973 cell-barcodes

with 11,385 median unique molecular identifiers (UMIs, transcripts) per cell and 3,076 median genes per cell sequenced to 71.0% sequencing saturation with 94,260 mean reads per cell for MAFIA mouse sample; 9,801 cell-barcodes with 13,467 median UMIs per cell and 3,211 median genes per cell sequenced to 74.9% sequencing saturation with 119,820 mean reads per cell for the first *Cd11c*^{YFP} mouse sample; 12,938 cell-barcodes with 14,439 median UMIs per cell and 3,199 median genes per cell sequenced to 71.4% sequencing saturation with 108,585 mean reads per cell for the second *Cd11c*^{YFP} mouse sample.

Analysis of scRNA-Seq

Preprocessing

The Scanpy[92] pipeline was used to read the count matrix. Three batches of samples (one from GFP^{+} cells from MAFIA mouse and two from YFP^{+} cells from *Cd11c*^{YFP} mice) were preprocessed independently and integrated later. Cells that expressed <200 genes and genes that were expressed in <3 cells were filtered out. The percentage of mitochondrial genes was calculated -and cells with >10% mitochondrial genes were removed. Cells with >7,000 genes or <1,000 genes were also removed. Read counts were normalized to library size 10,000 and log-transformed with scanpy.pp.log1p function.

Datasets integration and batch effect correction

Read count matrices and spliced/unspliced matrices were merged first. Principal Component Analysis was applied to reduce dimensions to 70. BBKNN[93] was then used to remove batch effects with the scanpy.external.pp.bbknn function with default parameters.

Visualization and clustering

UMAP[94] provided by scanpy was used to visualize data with default parameters. K-nearest neighbor and Leiden clustering were applied sequentially to cluster cells into groups. K-nearest neighbor graph construction was done by scanpy.pp.neighbors with parameters n_neighbors=12 and n_pcs=70. Leiden clustering was then performed by scanpy.tl.leiden with parameter resolution=0.15. To improve UMAP visualization, scanpy.tl.paga was applied, and we trimmed unnecessary graph edges by scanpy.tl.paga with threshold=0.018.

Marker genes and statistics

Wilcoxon rank-sum tests were applied to examine differentially expressed genes. Clusters were selected from the result of Leiden clustering. Differentially expressed genes of a cluster against other clusters were identified by scanpy.tl.rank_genes_groups and scanpy.pl.rank_genes_groups. P-values were collected for each cluster and transformed by negative $\log_{10}$ for better visualization. The top 50 differentially expressed genes were visualized in the figure.

Immunofluorescent staining

Dissected thymus lobes from C57BL/6 mice were cleaned of connective tissue and fixed in 4% paraformaldehyde (Sigma) for 1 h at 4˚C, washed in PBS, submerged in 10% sucrose, and then in 30% sucrose for 12 h each. The tissue was then frozen in Tissue-Tek OCT compound (Sakura Fintek) for cryostat sectioning. 10 or 20 µm thick sections were prepared with CryoStar NX50 (ThermoFisher) on Superfrost PLUS (ThermoScientific) microscope

slides, dried overnight, and stored at -80˚C until used. Before staining, the sections were fixed with acetone (Sigma) at -20˚C for 10 min, air-dried, then blocked with 5% goat serum + 5% donkey serum (both from Jackson Immunoresearch) in PBS for 2 h and stained with primary antibodies: rat monoclonal to MerTK (DS5MMER, eBioscience), rat monoclonal to TIM4 (RMT4-54, Bio-X-Cell), rabbit polyclonal to CD64 (Sinobiological), or rabbit polyclonal to Keratin 5 (BioLegend) overnight at 4˚C in a humidified chamber. After washing in PBS, the sections were labeled with goat anti-rat-Alexa Fluor 647 (Invitrogen) or goat anti-rat Cy3 (Jackson Immunoresearch) and donkey anti-rabbit Cy3 or donkey anti-rabbit AF647 (both from Jackson Immunoresearch) secondary antibodies for 2 hours at room temperature, followed by 5 min staining with DAPI. TUNEL Assay was done with the Click-iT Plus TUNEL Assay Alexa Fluor 647 kit (Invitrogen) according to the manufacturer's recommendations. A positive (pre-incubation with DNase I for 30 min at room temperature) and negative (no TdT enzyme) controls were always included. The sections were mounted with 0.1% n-propyl gallate (Sigma) in glycerol (Sigma) and imaged with an AxioObserver 7 (Carl Zeiss) wide-field microscope equipped with Plan Apochromat 20x NA=0.8 objective (Zeiss) and AxioCam 702 mono camera (Zeiss) and controlled by Zen 2.3 Blue (Zeiss) software. Image analysis was performed with Imaris 8.0.2 (Bitplane).

The co-localization scoring for MerTK and TIM4 with TUNEL was done with Imaris 8.2 (Bitplane). TUNEL$^+$ cells were detected with the Spots function, while MerTK$^+$ and TIM4$^+$ cells were detected with the Surface function. Spots

that co-localize with Surfaces were identified with the “Find Spots close to Surface” function of Imaris XT. The threshold for co-localization was set to 5 µm. The results were manually curated so that Spots categorized as “not co-localized” that were: 1) at the edge of the imaging field were excluded from consideration; 2) with clear Surface signal around them were re-categorized as "co-localized". The ratio of co-localized Spots to all Spots was calculated and presented as the co-localization index.

Thymus transplantation

To obtain E15.5 embryos, *SpiC*^{GFP} (CD45.2) homozygous male and congenic CD45.1 female mice were mated in a cage overnight and separated on the next day. Pregnant mice were sacrificed 15 days later, the viable embryos were harvested, and the thymuses were isolated in ice-cold PBS. C57BL/6 recipients were anesthetized by i.p injection of Ketamine hydrochloride (120 µg/g, Toronto Research Chemicals) and Xylazine hydrochloride (12 µg/g, Sigma). The fur on the left flank was removed, and the left kidney was exposed by cutting the skin, muscle layer, and peritoneum. The kidney capsule was nicked with a G23 needle, and the fetal thymus was pushed into the pocket under the kidney capsule with a G23 needle equipped with a plunger from a spinal needle. After the kidney was re-positioned back into the peritoneal cavity, the peritoneum was sutured, and the skin was stapled with metal clips. Rymadil (Carprofen, 5 µg/g, Zoetis) was given subcutaneously to ease the wound pain, and Trimerin (Sulfadiazine at 0.5 mg/mL + Trimethoprim at 0.1 mg/mL) were given in the drinking water for the first two weeks after the surgery. The metal clips were removed from the skin

after the first week, and the transplanted thymus and recipient's endogenous thymus were harvested and analyzed six weeks after the kidney transplantation.

Statistical analysis

Comparison between groups was made with Prism 6 (GraphPad Software). Comparisons between two groups were carried out with unpaired Student's t-test. When more than two groups were compared, a one-way ANOVA with Tukey correction was used. Differences were considered significant if $p<0.05$.

Data availability

The RNA Sequencing data of thymic macrophages and thymic dendritic cells are available at NCBI Gene Expression Omnibus (GEO) as part of GSE122108 and at www.immgen.org. The single cell RNA sequencing data is deposited at NCBI GEO under accession number GSE185460. The source data underlying Fig. 1H and I, Fig. 3B, D, and G, Fig. 5C, F, and I, Fig. 6B, F, and H, Fig. 7B, C, D, and G, Fig. 8B, D, E, and F, Fig. 1S5, Fig. 2S1, Fig. 2S2, Fig. 2S3, Fig. 5S1, and Fig. 5S2 are provided in the Source Data files. All other data supporting the findings of this study are available within the article and its figures and tables.

Abbreviations:

cDC – classical dendritic cell

DC – dendritic cell

EdU – 5-Ethynyl-2'-deoxyuridine

GO – gene ontology

HSC – hematopoietic stem cell

IFN-I – type I Interferon

IMMGEN – Immunological Genome Consortium

scRNA-Seq – single-cell RNA sequencing

TF – transcription factor

ThyMacs – thymic macrophages

TRA – tissue-restricted antigen

YS – yolk sac

References:

1. Wynn TA, Chawla A, Pollard JW. Macrophage biology in development, homeostasis and disease. Nature; 2013;496: 445–455. doi:10.1038/nature12034

2. Baratin M, Simon L, Jorquera A, Ghigo C, Dembele D, Nowak J, et al. T Cell Zone Resident Macrophages Silently Dispose of Apoptotic Cells in the Lymph Node. Immunity; 2017;47: 349–362.e5. doi:10.1016/j.immuni.2017.07.019

3. A-Gonzalez N, Castrillo A. Origin and Specialization of Splenic Macrophages. Cellular Immunology. 2018;330: 1–27. doi:10.1016/j.cellimm.2018.05.005

4. Bellomo A, Mondor I, Spinelli L, Lagueyrie M, Stewart BJ, Brouilly N, et al. Reticular Fibroblasts Expressing the Transcription Factor WT1 Define a Stromal Niche that Maintains and Replenishes Splenic Red Pulp Macrophages. Immunity; 2020;53: 127–142.e7. doi:10.1016/j.immuni.2020.06.008

5. van Furth R, Cohn ZA. The origin and kinetics of mononuclear phagocytes. J Exp Med; 1968;128: 415–435. doi:10.1084/jem.128.3.415

6. Ginhoux F, Guilliams M. Tissue-Resident Macrophage Ontogeny and Homeostasis. Immunity. 2016;44: 439–449. doi:10.1016/j.immuni.2016.02.024

7. Perdiguero EG, Klapproth K, Schulz C, Busch K, Azzoni E, Crozet L, et al. Tissue-resident macrophages originate from yolk-sac-derived

erythro-myeloid progenitors. Nat Immunol; 2015;518: 547–551. doi:10.1038/nature13989

8. Mass E, Ballesteros I, Farlik M, Halbritter F, Günther P, Crozet L, et al. Specification of tissue-resident macrophages during organogenesis. Science; 2016;353: aaf4238–aaf4238. doi:10.1126/science.aaf4238

9. Ginhoux F, Greter M, Leboeuf M, Nandi S, See P, Gokhan S, et al. Fate mapping analysis reveals that adult microglia derive from primitive macrophages. Science. 2010;330: 841–845. doi:10.1126/science.1194637

10. Hoeffel G, Wang Y, Greter M, See P, Teo P, Malleret B, et al. Adult Langerhans cells derive predominantly from embryonic fetal liver monocytes with a minor contribution of yolk sac–derived macrophages. J Exp Med. 2012;209: 1167–1181. doi:10.1084/jem.20120340

11. Hoeffel G, Chen J, Lavin Y, Low D, Almeida FF, See P, et al. C-Myb(+) erythro-myeloid progenitor-derived fetal monocytes give rise to adult tissue-resident macrophages. Immunity. 2015;42: 665–678. doi:10.1016/j.immuni.2015.03.011

12. Goldmann T, Wieghofer P, Jordão MJC, Prutek F, Hagemeyer N, Frenzel K, et al. Origin, fate and dynamics of macrophages at central nervous system interfaces. Nat Immunol. 2016;17: 797–805. doi:10.1038/ni.3423

13. Hashimoto D, Chow A, Noizat C, Teo P, Beasley MB, Leboeuf M, et al. Tissue-Resident Macrophages Self-Maintain Locally throughout Adult Life with Minimal Contribution from Circulating Monocytes. Immunity; 2013;38: 792–804. doi:10.1016/j.immuni.2013.04.004

14. Epelman S, Lavine KJ, Beaudin AE, Sojka DK, Carrero JA, Calderon B, et al. Embryonic and Adult-Derived Resident Cardiac Macrophages Are Maintained through Distinct Mechanisms at Steady State and during Inflammation. Immunity; 2014;40: 91–104. doi:10.1016/j.immuni.2013.11.019

15. Sheng J, Ruedl C, Karjalainen K. Most Tissue-Resident Macrophages Except Microglia Are Derived from Fetal Hematopoietic Stem Cells. Immunity; 2015;43: 382–393. doi:10.1016/j.immuni.2015.07.016

16. Liu Z, Gu Y, Chakarov S, Bleriot C, Kwok I, Chen X, et al. Fate Mapping via Ms4a3-Expression History Traces Monocyte-Derived Cells. Cell; 2019;178: 1509–1525.e19. doi:10.1016/j.cell.2019.08.009

17. Ensan S, Li A, Besla R, Degousee N, Cosme J, Roufaiel M, et al. Self-renewing resident arterial macrophages arise from embryonic CX3CR1+ precursors and circulating monocytes immediately after birth. Nat Immunol; 2015;17: 159–168. doi:10.1038/ni.3343

18. Mondor I, Baratin M, Lagueyrie M, Saro L, Henri S, Gentek R, et al.

Lymphatic Endothelial Cells Are Essential Components of the Subcapsular Sinus Macrophage Niche. Immunity; 2019;50: 1453–1466.e4. doi:10.1016/j.immuni.2019.04.002

19. Molawi K, Wolf Y, Kandalla PK, Favret J, Hagemeyer N, Frenzel K, et al. Progressive replacement of embryo-derived cardiac macrophages with age. J Exp Med. 2014;211: 2151–2158. doi:10.1084/jem.20140639

20. Heidt T, Courties G, Dutta P, Sager HB, Sebas M, Iwamoto Y, et al. Differential Contribution of Monocytes to Heart Macrophages in Steady-State and After Myocardial Infarction. Circulation Research. 2014;115: 284–295. doi:10.1161/CIRCRESAHA.115.303567

21. Yahara Y, Barrientos T, Tang YJ, Puviindran V, Nadesan P, Zhang H, et al. Erythromyeloid progenitors give rise to a population of osteoclasts that contribute to bone homeostasis and repair. Nat Cell Biol; 2020;22: 1–28. doi:10.1038/s41556-019-0437-8

22. Jacome-Galarza CE, Percin GI, Muller JT, Mass E, Lazarov T, Eitler J, et al. Developmental origin, functional maintenance and genetic rescue of osteoclasts. Nature; 2019;568: 541–545. doi:10.1038/s41586-019-1105-7

23. Calderon B, Carrero JA, Ferris ST, Sojka DK, Moore L, Epelman S, et al. The pancreas anatomy conditions the origin and properties of resident macrophages. J Exp Med. 2015;212: 1497–1512. doi:10.1084/jem.20150496

24. Tamoutounour S, Guilliams M, Sanchis FM, Liu H, Terhorst D, Malosse C, et al. Origins and Functional Specialization of Macrophages and of Conventional and Monocyte-Derived Dendritic Cells in Mouse Skin. Immunity; 2013;39: 925–938. doi:10.1016/j.immuni.2013.10.004

25. Bain CC, Bravo-Blas A, Scott CL, Gomez Perdiguero E, Geissmann F, Henri S, et al. Constant replenishment from circulating monocytes maintains the macrophage pool in the intestine of adult mice. Nat Immunol. 2014;15: 929–937. doi:10.1038/ni.2967

26. Sierro F, Evrard M, Rizzetto S, Melino M, Mitchell AJ, Florido M, et al. A Liver Capsular Network of Monocyte-Derived Macrophages Restricts Hepatic Dissemination of Intraperitoneal Bacteria by Neutrophil Recruitment. Immunity; 2017;47: 374–388.e6. doi:10.1016/j.immuni.2017.07.018

27. Mossadegh-Keller N, Gentek R, Gimenez G, Bigot S, Mailfert S, Sieweke MH. Developmental origin and maintenance of distinct testicular macrophage populations. J Exp Med. 2017;214: 2829–2841. doi:10.1084/jem.20170829

28. Lokka E, Lintukorpi L, Cisneros-Montalvo S, Mäkelä J-A, Tyystjärvi S, Ojasalo V, et al. Generation, localization and functions of macrophages

during the development of testis. Nature Communications. Springer US; 2020;11: 1–16. doi:10.1038/s41467-020-18206-0

29. Wang M, Yang Y, Cansever D, Wang Y, Kantores C, Messiaen S, et al. Two populations of self-maintaining monocyte-independent macrophages exist in adult epididymis and testis. PNAS. 2020;118: e2013686117. doi:10.1073/pnas.2013686117/-/DCSupplemental

30. Bain CC, Hawley CA, Garner H, Scott CL, Schridde A, Steers NJ, et al. Long-lived self-renewing bone marrow-derived macrophages displace embryo-derived cells to inhabit adult serous cavities. Nature Communications; 2016;7: 1–14. doi:10.1038/ncomms11852

31. Surh CD, Sprent J. T-cell apoptosis detected in situ during positive and negative selection in the thymus. Nature. 1994;372: 100–103. doi:10.1038/372100a0

32. Esashi E, Sekiguchi T, Ito H, Koyasu S, Miyajima A. Cutting Edge: A possible role for CD4+ thymic macrophages as professional scavengers of apoptotic thymocytes. Journal of Immunology; 2003;171: 2773–2777. doi:10.4049/jimmunol.171.6.2773

33. Liu L-T, Lang Z-F, Li Y, Zhu Y-J, Zhang J-T, Guo S-F, et al. Composition and characteristics of distinct macrophage subpopulations in the mouse thymus. Molecular Medicine Reports. 2013;7: 1850–1854. doi:10.3892/mmr.2013.1448

34. Guerri L, Peguillet I, Geraldo Y, Nabti S, Premel V, Lantz O. Analysis of APC types involved in CD4 tolerance and regulatory T cell generation using reaggregated thymic organ cultures. J Immunol; 2013;190: 2102–2110. doi:10.4049/jimmunol.1202883

35. Lopes N, Charaix J, Cédile O, Sergé A, Irla M. Lymphotoxin alpha fine-tunes T cell clonal deletion by regulating thymic entry of antigen-presenting cells. Nature Communications; 2018;9: 1–16. doi:10.1038/s41467-018-03619-9

36. Kim H-J, Alonzo ES, Dorothee G, Pollard JW, Sant'Angelo DB. Selective depletion of eosinophils or neutrophils in mice impacts the efficiency of apoptotic cell clearance in the thymus. PLoS ONE. 2010;5: e11439. doi:10.1371/journal.pone.0011439.g010

37. Tacke R, Hilgendorf I, Garner H, Waterborg C, Park K, Nowyhed H, et al. The transcription factor NR4A1 is essential for the development of a novel macrophage subset in the thymus. Sci Rep. 2015;5: 10055. doi:10.1038/srep10055

38. Gautier EL, Shay T, Miller J, Greter M, Jakubzick C, Ivanov S, et al. Gene-expression profiles and transcriptional regulatory pathways that underlie the identity and diversity of mouse tissue macrophages. Nat Immunol. 2012;13: 1118–1128. doi:10.1038/ni.2419

39. Ingersoll MA, Spanbroek R, Lottaz C, Gautier EL, Frankenberger M, Hoffmann R, et al. Comparison of gene expression profiles between human and mouse monocyte subsets. Blood. 2010;115: e10–e19. doi:10.1182/blood-2009-07-235028

40. Wang H, Breed ER, Lee YJ, Qian LJ, Jameson SC, Hogquist KA. Myeloid cells activate iNKT cells to produce IL-4 in the thymic medulla. Proc Natl Acad Sci; 2019;116: 22262–22268. doi:10.1073/pnas.1910412116

41. Chan CT, Fenn AM, Harder NK, Mindur JE, McAlpine CS, Patel J, et al. Liver X receptors are required for thymic resilience and T cell output. J Exp Med. 2020;217: 245–23. doi:10.1084/jem.20200318

42. Wada H, Masuda K, Satoh R, Kakugawa K, Ikawa T, Katsura Y, et al. Adult T-cell progenitors retain myeloid potential. Nature; 2008;452: 768–772. doi:10.1038/nature06839

43. Bell JJ, Bhandoola A. The earliest thymic progenitors for T cells possess myeloid lineage potential. Nature. 2008;452: 764–767. doi:10.1038/nature06840

44. Schlenner SM, Madan V, Busch K, Tietz A, LAufle C, Costa C, et al. Fate Mapping Reveals Separate Origins of T Cells and Myeloid Lineages in the Thymus. Immunity; 2010;32: 426–436. doi:10.1016/j.immuni.2010.03.005

45. Witmer-Pack MD, Hughes DA, Schuler G, Lawson L, McWilliam A, Inaba K, et al. Identification of macrophages and dendritic cells in the osteopetrotic (op/op) mouse. J Cell Sci. 1993;104 (Pt 4): 1021–1029.

46. Sasmono RT, Oceandy D, Pollard JW, Tong W, Pavli P, Wainwright BJ, et al. A macrophage colony-stimulating factor receptor-green fluorescent protein transgene is expressed throughout the mononuclear phagocyte system of the mouse. Blood; 2003;101: 1155–1163. doi:10.1182/blood-2002-02-0569

47. Hume DA. Applications of myeloid-specific promoters in transgenic mice support in vivo imaging and functional genomics but do not support the concept of distinct macrophage and dendritic cell lineages or roles in immunity. Journal of Leukocyte Biology. 2011;89: 525–538. doi:10.1189/jlb.0810472

48. Taniuchi I, Osato M, Egawa T, Sunshine MJ, Bae SC, Komori T, et al. Differential requirements for Runx proteins in CD4 repression and epigenetic silencing during T lymphocyte development. Cell. 2002;111: 621–633. doi:10.1016/s0092-8674(02)01111-x

49. Ebihara T, Song C, Ryu SH, Plougastel-Douglas B, Yang L, Levanon D, et al. Runx3 specifies lineage commitment of innate lymphoid cells. Nat Immunol; 2015;16: 1124–1133. doi:10.1038/ni.3272

50. Fainaru O, Woolf E, Lotem J, Yarmus M, Brenner O, Goldenberg D, et al. Runx3 regulates mouse TGF-beta-mediated dendritic cell function and its absence results in airway inflammation. EMBO J; 2004;23: 969–979. doi:10.1038/sj.emboj.7600085

51. Kohyama M, Ise W, Edelson BT, Wilker PR, Hildner K, Mejia C, et al. Role for Spi-C in the development of red pulp macrophages and splenic iron homeostasis. Nat Immunol; 2008;457: 318–321. doi:10.1038/nature07472

52. Haldar M, Kohyama M, So AY-L, KC W, Wu X, Briseño CG, et al. Heme-Mediated SPI-C Induction Promotes Monocyte Differentiation into Iron-Recycling Macrophages. Cell; 2014;156: 1223–1234. doi:10.1016/j.cell.2014.01.069

53. Yona S, Kim K-W, Wolf Y, Mildner A, Varol D, Breker M, et al. Fate Mapping Reveals Origins and Dynamics of Monocytes and Tissue Macrophages under Homeostasis. Immunity; 2013;38: 79–91. doi:10.1016/j.immuni.2012.12.001

54. McCaughtry TM, Wilken MS, Hogquist KA. Thymic emigration revisited. J Exp Med. 2007;204: 2513–2520. doi:10.1084/jem.20070601

55. Lienenklaus S, Cornitescu M, Ziętara N, Łyszkiewicz M, Gekara N, Jabłónska J, et al. Novel reporter mouse reveals constitutive and inflammatory expression of IFN-beta in vivo. J Immunol; 2009;183: 3229–3236. doi:10.4049/jimmunol.0804277

56. Otero DC, Baker DP, David M. IRF7-dependent IFN-β production in response to RANKL promotes medullary thymic epithelial cell development. J Immunol; 2013;190: 3289–3298. doi:10.4049/jimmunol.1203086

57. Breed ER, Lee ST, Hogquist KA. Directing T cell fate: How thymic antigen presenting cells coordinate thymocyte selection. Seminars in Cell and Developmental Biology; 2017;: 1–9. doi:10.1016/j.semcdb.2017.07.045

58. Kurd NS, Lutes LK, Yoon J, Chan SW, Dzhagalov IL, Hoover AR, et al. A role for phagocytosis in inducing cell death during thymocyte negative selection. eLife. 2019;8: 1879–18. doi:10.7554/eLife.48097

59. Morioka S, Perry JSA, Raymond MH, Medina CB, Zhu Y, Zhao L, et al. Efferocytosis induces a novel SLC program to promote glucose uptake and lactate release. Nature; 2018;563: 1–21. doi:10.1038/s41586-018-0735-5

60. Bleriot C, Chakarov S, Ginhoux F. Determinants of Resident Tissue Macrophage Identity and Function. Immunity; 2020;52: 957–970. doi:10.1016/j.immuni.2020.05.014

61. Stritesky GL, Xing Y, Erickson JR, Kalekar LA, Wang X, Mueller DL, et

al. Murine thymic selection quantified using a unique method to capture deleted T cells. Proc Natl Acad Sci. 2013;110: 4679–4684. doi:10.1073/pnas.1217532110

62. Baba T, Nakamoto Y, Mukaida N. Crucial Contribution of Thymic Sirp + Conventional Dendritic Cells to Central Tolerance against Blood-Borne Antigens in a CCR2-Dependent Manner. J Immunol. 2009;183: 3053–3063. doi:10.4049/jimmunol.0900438

63. Gallegos AM, Bevan MJ. Central Tolerance to Tissue-specific Antigens Mediated by Direct and Indirect Antigen Presentation. J Exp Med. 2004;200: 1039–1049. doi:10.1084/jem.20041457

64. Koble C, Kyewski B. The thymic medulla: a unique microenvironment for intercellular self-antigen transfer. J Exp Med. 2009;206: 1505–1513. doi:10.1084/jem.20082449

65. Vobořil M, Brabec T, Dobeš J, Šplíchalová I, Březina J, Čepková A, et al. Toll-like receptor signaling in thymic epithelium controls monocyte-derived dendritic cell recruitment and Treg generation. Nature Communications; 2020;11: 1–16. doi:10.1038/s41467-020-16081-3

66. Dixit VD. Impact of immune-metabolic interactions on age-related thymic demise and T cell senescence. Semin Immunol; 2012;24: 321–330. doi:10.1016/j.smim.2012.04.002

67. Rivera-Gonzalez GC, Shook BA, Andrae J, Holtrup B, Bollag K, Betsholtz C, et al. Skin Adipocyte Stem Cell Self-Renewal Is Regulated by a PDGFA/AKT-Signaling Axis. Stem Cell; 2016;19: 738–751. doi:10.1016/j.stem.2016.09.002

68. Olson LE, Soriano P. Increased PDGFRα Activation Disrupts Connective Tissue Development and Drives Systemic Fibrosis. Developmental Cell; 2009;16: 303–313. doi:10.1016/j.devcel.2008.12.003

69. Satpathy AT, KC W, Albring JC, Edelson BT, Kretzer NM, Bhattacharya D, et al. Zbtb46expression distinguishes classical dendritic cells and their committed progenitors from other immune lineages. J Exp Med. 2012;209: 1135–1152. doi:10.1084/jem.20120030

70. Guilliams M, Mildner A, Yona S. Developmental and Functional Heterogeneity of Monocytes. Immunity; 2018;49: 595–613. doi:10.1016/j.immuni.2018.10.005

71. Tabula Muris Consortium. Single-cell transcriptomics of 20 mouse organs creates a Tabula Muris. Nature; 2018;562: 367–372. doi:10.1038/s41586-018-0590-4

72. Han X, Wang R, Zhou Y, Fei L, Sun H, Lai S, et al. Mapping the Mouse Cell Atlas by Microwell-Seq. Cell; 2018;172: 1091–1097.e17. doi:10.1016/j.cell.2018.02.001

73. Tabula Muris Consortium. A single-cell transcriptomic atlas characterizes ageing tissues in the mouse. Nature; 2020;583: 590–595. doi:10.1038/s41586-020-2496-1

74. Kernfeld EM, Genga RMJ, Neherin K, Magaletta ME, Xu P, Maehr R. A Single-Cell Transcriptomic Atlas of Thymus Organogenesis Resolves Cell Types and Developmental Maturation. Immunity; 2018;: 1–33. doi:10.1016/j.immuni.2018.04.015

75. Park J-E, Botting RA, Domínguez Conde C, Popescu D-M, Lavaert M, Kunz DJ, et al. A cell atlas of human thymic development defines T cell repertoire formation. Science; 2020;367: eaay3224–12. doi:10.1126/science.aay3224

76. Bornstein C, Nevo S, Giladi A, Kadouri N, Pouzolles M, Gerbe F, et al. Single-cell mapping of the thymic stroma identifies IL-25-producing tuft epithelial cells. Nature; 2018;559:1–25. doi:10.1038/s41586-018-0346-1

77. Bautista JL, Cramer NT, Miller CN, Chavez J, Berrios DI, Byrnes LE, et al. Single-cell transcriptional profiling of human thymic stroma uncovers novel cellular heterogeneity in the thymic medulla. Nature Communications; 2021;12: 1096–15. doi:10.1038/s41467-021-21346-6

78. Burnett SH, Kershen EJ, Zhang J, Zeng L, Straley SC, Kaplan AM, et al. Conditional macrophage ablation in transgenic mice expressing a Fas-based suicide gene. Journal of Leukocyte Biology; 2004;75: 612–623. doi:10.1189/jlb.0903442

79. Jung S, Aliberti J, Graemmel P, Sunshine MJ, Kreutzberg GW, Sher A, et al. Analysis of fractalkine receptor CX(3)CR1 function by targeted deletion and green fluorescent protein reporter gene insertion. Mol Cell Biol. 2000;20: 4106–4114.

80. Lindquist RL, Shakhar G, Dudziak D, Wardemann H, Eisenreich T, Dustin ML, et al. Visualizing dendritic cell networks in vivo. Nat Immunol. 2004;5: 1243–1250. doi:10.1038/ni1139

81. Faust N, Varas F, Kelly LM, Heck S, Graf T. Insertion of enhanced green fluorescent protein into the lysozyme gene creates mice with green fluorescent granulocytes and macrophages. Blood. 2000;96: 719–726.

82. Roesch K, Jadhav AP, Trimarchi JM, Stadler MB, Roska B, Sun BB, et al. The transcriptome of retinal Müller glial cells. J Comp Neurol. 2008;509: 225–238. doi:10.1002/cne.21730

83. Madisen L, Zwingman TA, Sunkin SM, Oh SW, Zariwala HA, Gu H, et al. A robust and high-throughput Cre reporting and characterization system for the whole mouse brain. Nature Neuroscience; 2009;13: 133–140. doi:10.1038/nn.2467

84. Picelli S, Faridani OR, rklund ASKBO, Winberg GOS, Sagasser S,

Sandberg R. Full-length RNA-seq from single cells using Smart-seq2. Nature Protocols; 2014;9: 171–181. doi:10.1038/nprot.2014.006

85. Picelli S, Björklund ÅK, Faridani OR, Sagasser S, Winberg G, Sandberg R. Smart-seq2 for sensitive full-length transcriptome profiling in single cells. Nat Meth. 2013;10: 1096–1098. doi:10.1038/nmeth.2639

86. Love MI, Huber W, Anders S. Moderated estimation of fold change and dispersion for RNA-seq data with DESeq2. Genome Biol. BioMed Central; 2014;15: 31–21. doi:10.1186/s13059-014-0550-8

87. Schmeier S, Alam T, Essack M, Bajic VB. TcoF-DB v2: update of the database of human and mouse transcription co-factors and transcription factor interactions. Nucleic Acids Res. 2017;45: D145–D150. doi:10.1093/nar/gkw1007

88. Reich M, Liefeld T, Gould J, Lerner J, Tamayo P, Mesirov JP. GenePattern 2.0. Nat Genet; 2006;38: 500–501. doi:10.1038/ng0506-500

89. Yu G, Wang L-G, Han Y, He Q-Y. clusterProfiler: an R Package for Comparing Biological Themes Among Gene Clusters. OMICS: A Journal of Integrative Biology; 2012;16: 284–287. doi:10.1089/omi.2011.0118

90. Heyne GW, Plisch EH, Melberg CG, Sandgren EP, Peter JA, Lipinski RJ. A Simple and Reliable Method for Early Pregnancy Detection in Inbred Mice. J Am Assoc Lab Anim Sci. 2015;54: 368–371.

91. Iturri L, Saenz Coronilla J, Lallemand Y, Gomez Perdiguero E. Identification Of Erythromyeloid Progenitors And Their Progeny In The Mouse Embryo By Flow Cytometry. JoVE. 2017;: 1–10. doi:10.3791/55305

92. Wolf FA, Angerer P, Theis FJ. SCANPY: large-scale single-cell gene expression data analysis. Genome Biol; 2018;19: 15–5. doi:10.1186/s13059-017-1382-0

93. Polański K, Young MD, Miao Z, Meyer KB, Teichmann SA, Park J-E. BBKNN: fast batch alignment of single cell transcriptomes. Bioinformatics. 2019;36: 964–965. doi:10.1093/bioinformatics/btz625#supplementary-data

94. McInnes L, Healy J, Melville J. UMAP: Uniform Manifold Approximation and Projection for Dimension Reduction. ArXiv e-prints. 2018. doi:1802.03426v3

Acknowledgments

We are grateful to the IMMGEN consortium for performing the RNA sequencing of our samples and providing access to its database. We thank the following core facilities at National Yang Ming Chiao Tung University: Instrumentation Resource Center for providing access to its sorting and imaging facility and the Animal Facility for mouse husbandry. We are very grateful to Wan-Chun Chang, Bing-Xiu Guo, Chien-Yi Tung, and Kate Hua from the Genomics Center for Clinical and Biotechnological Applications of NCFB (NYCU, Taipei) for help with scRNA-Seq. Special thanks go to Dr. Fang Liao, Academia Sinica, Taipei, for help with cell sorting and for providing the 24G2 hybridoma, and Chang-Feng Chu for technical assistance. We are very grateful to Alexandra Norris, Cecilia Tai, and Angelina Shih for the manual scoring of the in vitro phagocytosis experiments. We are indebted to Dr. Yu-Wen Su (NHRI, Taiwan) for help with the mice. Some figures were made with BioRender.

This work was supported by the Ministry of Science and Technology, Taiwan (grants # 107-2320-B-010 -016 -MY3, 110-2320-B-A49A-521 - , and 111-2320-B-A49 -031 -MY3 to IL Dzhagalov), the Yen-Tjing Ling Medical Foundation (grant # CI-111-6 to IL Dzhagalov), and the Cancer Progression Research Center (NYCU). The authors declare no competing financial interests.

Author contributions

TA Zhou designed experiments, performed research, analyzed and interpreted data, and wrote the manuscript; HP Hsu, HK Cheng, and CY Lin performed research, analyzed and interpreted data; YH Tu and HC Huang

analyzed the scRNA-Seq data; NJ Chen, JW Tsai, EA Robey, and CL Hsu provided expertise, shared critical reagents, and edited the manuscript; IL Dzhagalov conceptualized the studies, designed experiments, performed research, analyzed, interpreted the data, and wrote the manuscript.

Supplementary figures and tables

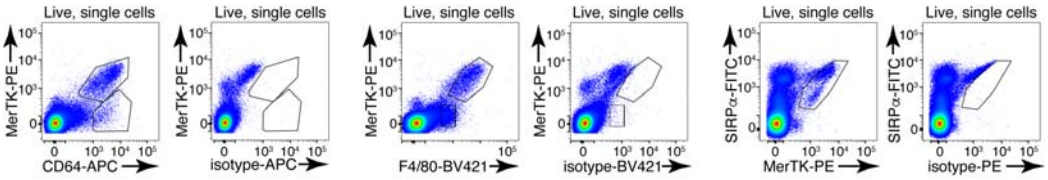

Figure 1 – figure supplement 1: Representative flow cytometry staining of enzymatically digested thymus single-cell suspension for CD64, MerTK, and F4/80 and respective isotype controls. The flow cytometry plots are representative of 5 individual experiments.

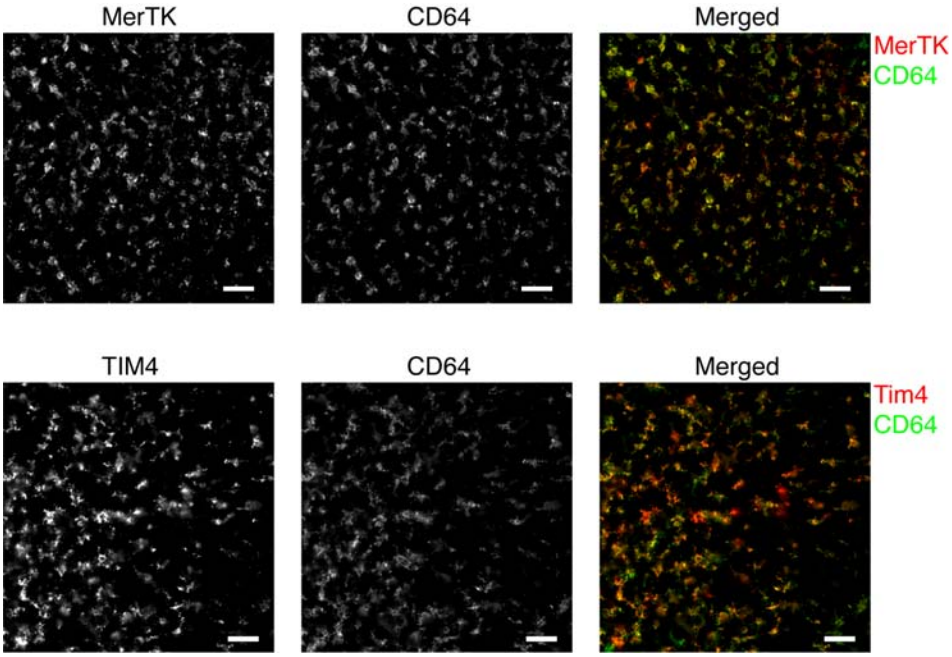

Figure 1 – figure supplement 2: Immunofluorescent images of thymic sections showing co-localization of MerTK and CD64 staining (upper row) and TIM4 and CD64 staining (lower row) in the thymic cortex. The images are representative of at least three mice. The scale bar is 50 µm.

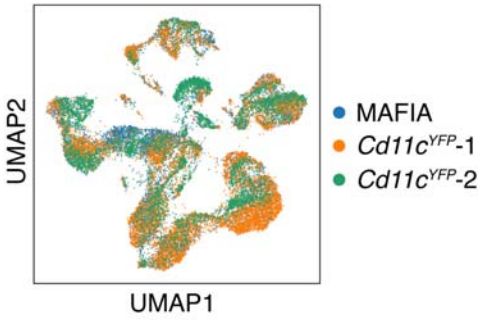

Figure 1 – figure supplement 3: UMAP clustering of the scRNA-Seq data shows that the cells from the three samples (one from GFP^+ cells in MAFIA mice and two from YFP^+ cells in *Cd11c*^{YFP} mice) overlap considerably.

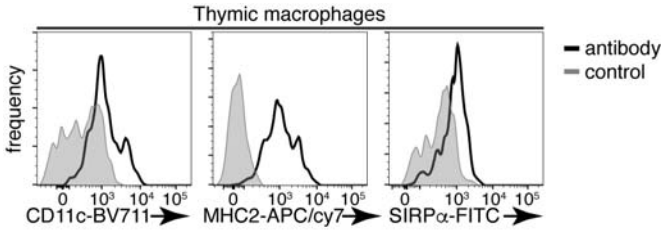

Figure 1 – figure supplement 4: Expression of CD11c, MHC2, and SIRPα on ThyMacs with respective controls. The flow cytometry plots are representative of 5 individual experiments.

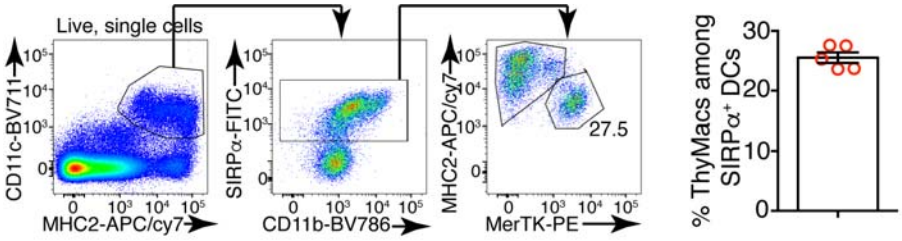

Figure 1 – figure supplement 5: Example flow cytometry plots showing that gating on CD11c^{+}MHC2^{+} thymus cells, in addition to DCs, also includes macrophages, especially among SIRPα^{+} cells. On the right is a plot of the frequency of MerTK^{+} cells among CD11c^{+}MHC2^{+}SIRPα^{+} cells. The data are mean±SEM from 5 individual mice. Each dot is an individual mouse. The numbers in the flow cytometry plots are the percent of cells in the respective gate.

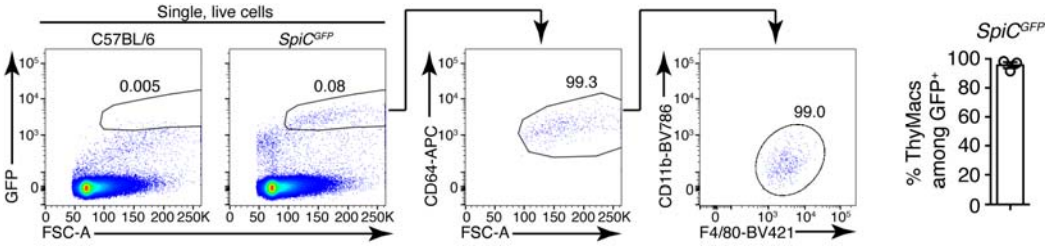

Figure 2 – figure supplement 1: Example of the gating strategy to identify ThyMacs among *Spic*$^{GFP+}$ cells. On the right is a plot showing the mean±SEM of the frequencies of ThyMacs among *Spic*$^{GFP+}$ cells. Each dot is an individual mouse. The numbers in the flow cytometry plots are the percent of cells in the respective gate.

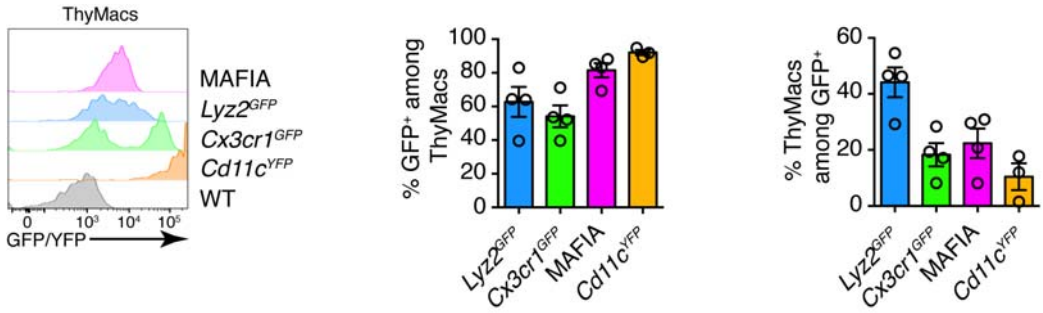

Figure 2 – figure supplement 2: Representative flow cytometry plots of the expression of four reporter alleles in ThyMacs (left), frequencies of GFP/YFP^{+} cells among ThyMacs (middle), and frequencies of ThyMacs among GFP/YFP^{+} cells (right). Data in the graphs represent mean±SEM. Each dot is an individual mouse.

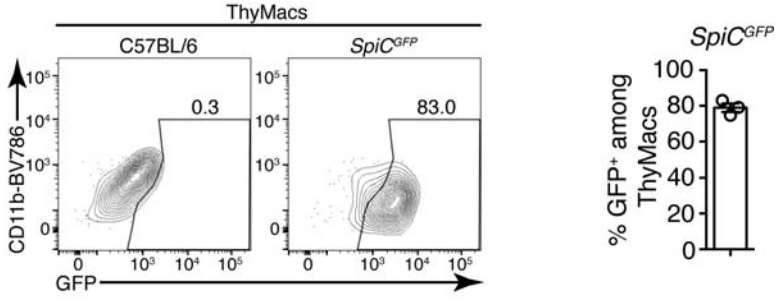

Figure 2 – figure supplement 3: Representative flow cytometry plots of the expression of *Spic*^{GFP} in ThyMacs. To the right is a graph showing the mean±SEM of the frequencies of *Spic*$^{GFP+}$ cells among ThyMacs. Each dot is an individual mouse. The numbers in the flow cytometry plots are the percent of cells in the respective gate.

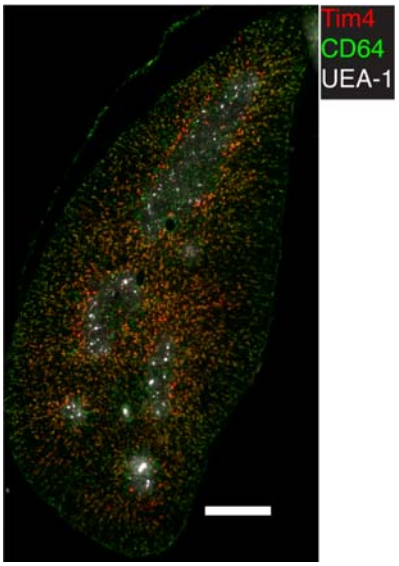

Figure 4 figure supplement 1: Representative immunofluorescent image of WT thymic frozen section stained for TIM4, CD64, and UEA-1 (a marker for medulla). CD64 stains all macrophages, while TIM4 – only a subset that is located in the cortex. The image is representative of 3 mice. The scale bar is 400 µm.

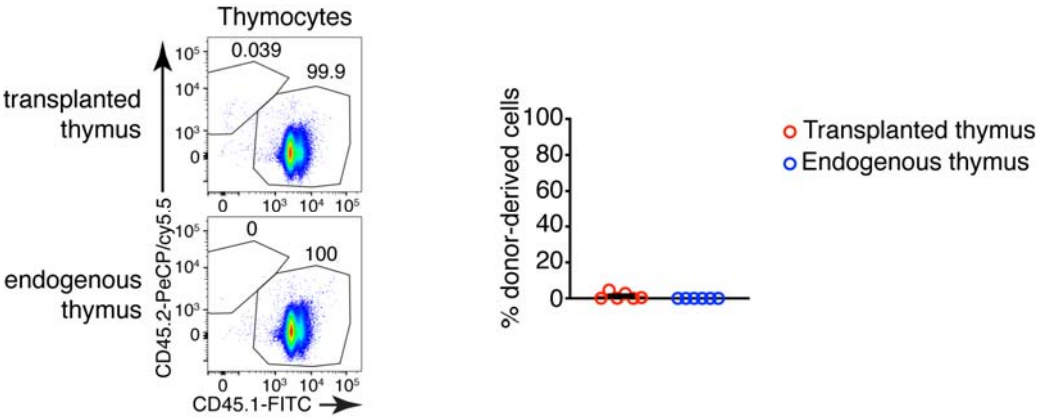

Figure 5 – figure supplement 1: Representative flow cytometry plots of donor (CD45.2$^+$) vs. host (CD45.1$^+$) derived thymocytes in the transplanted thymus. The host thymus (endogenous thymus) serves as a negative control. To the right is a graph showing the mean±SEM of the frequencies of CD45.2$^+$ (donor-derived) cells among thymocytes in the transplanted and endogenous

thymuses of the mice. Each dot is an individual mouse. The numbers in the flow cytometry plots are the percent of cells in the respective gate.

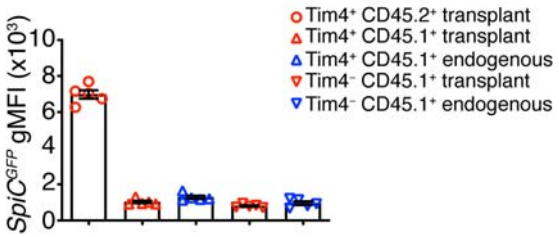

Figure 5 – figure supplement 2: Comparison of the geometric mean fluorescent intensities (gMFI) of SpiC^{GFP} TIM4^{+} and TIM4^{-} thymic macrophages of host and donor-origin in the transplanted thymus. The endogenous thymus serves as background control. Only populations comprising >5% of thymic macrophages are shown. Each dot is an individual mouse. The data are presented as mean±SEM.

Table 1: Expression of differentially up-regulated transcription factors in thymic macrophages

Gene name	ThyMacs	non-ThyMacs
Irf7	3879.32	300.82
Irf8	3528.27	1474.35
Stat1	2403.69	522.04
Dnmt3a	1515.94	647.81
Znxf1	1379.89	635.36
Stat2	1210.35	472.53
Nr1h3	1182.17	147.05
Srebf1	975.09	399.06
Rxra	760.26	298.55
Trps1	746.36	232.48
Runx3	723.14	9.76
Relb	715.53	293.92
Sp100	696.94	324.47
Zbp1	639.19	69.83
Tfec	588.72	74.66
Spic	573.11	34.36
Nfkbie	569.74	226.76

Ncoa4	550.69	249.15
Rest	548.22	269.22
Meis3	530.8	120.91
Bhlhe40	490.59	99.56
Parp12	414.11	126.82
Arid5b	374.03	177.08
Creb5	295.14	47.91
Pparg	276.54	33.24

Table 2: Expression of differentially up-regulated transcription factors in thymic macrophages. Transcription factors that were highly expressed in thymic macrophages (>250) and up-regulated >2-fold in thymic macrophages compared to non-thymic macrophages were listed alphabetically, and the geometric means of 4 replicates of thymic macrophages (ThyMacs) and two replicates of each of the 9 non-thymic macrophage populations (non-ThyMacs) were recorded. Non-thymic macrophages are: spleen red pulp macrophages, Kupffer cells, broncho-alveolar lavage macrophages, peritoneal cavity macrophages, aorta macrophages, heart macrophages, white adipose tissue macrophages, central nervous system microglia, spinal cord macrophages.

Table 2: List of the differentially expressed genes among *Timd*4+ thymic macrophages, *Cx3cr1*+ thymic macrophages, and thymic monocytes

***Cx3cr1*+ ThyMacs**		***Timd4*+ ThyMacs**		**ThyMonos**	
Gene name	adjusted p-value	Gene name	adjusted p-value	Gene name	adjusted p-value
Ctsz	0	*Hpgd*	0	*Alox5ap*	0
Cd63	0	*Serpinb6a*	0	*S100a6*	0
Pmepa1	0	*Slc40a1*	0	*Ly6c2*	0
Zmynd15	0	*Cd81*	0	*Ifi27l2a*	0
Olfml3	0	*Vcam1*	0	*Fau*	0
Mmp2	0	*Cfp*	0	*Coro1a*	0
AU020206	1.60E-290	*Spic*	0	*Ccr2*	0
Plxnd1	1.59E-285	*Trf*	0	*Rps27*	0
Cst7	8.68E-279	*Actn1*	0	*Tmsb10*	0
Dnase1l3	2.45E-270	*Maf*	0	*Ifitm2*	7.21E-302
Timp2	2.15E-267	*Pld3*	0	*Fxyd5*	6.36E-299

Lgals3bp	8.69E-263	*Il18*	0	*Rps19*	2.04E-292
Pdgfa	6.87E-255	*Mrc1*	0	*Rpl18*	6.50E-291
Mmp14	2.33E-253	*Crip2*	0	*Rpl9*	1.11E-289
Fam46c	9.99E-235	*Tmem65*	0	*Rps23*	1.28E-289
Chst2	1.19E-226	*Igf1*	0	*Napsa*	8.91E-279
Cp	5.36E-225	*Epb41l3*	0	*Ms4a4c*	8.25E-272
Camk1	7.12E-225	*Timd4*	0	*Plac8*	2.10E-270
B2m	1.09E-222	*Blvrb*	0	*Rpl18a*	9.26E-269
Lhfpl2	4.52E-217	*Clec1b*	0	*S100a4*	4.98E-268
Acp5	5.90E-216	*Cd68*	0	*Cd52*	3.67E-267
Lag3	3.91E-213	*Axl*	0	*Rps14*	1.94E-266
Lyz2	1.28E-209	*Paqr9*	3.32E-307	*Ifitm3*	3.19E-263
H2-M2	1.22E-199	*Sdc3*	3.45E-305	*Rpl34*	2.02E-261
Psap	7.26E-198	*Myo9a*	5.59E-305	*Rps27a*	3.67E-260
Gatm	1.33E-192	*Scp2*	3.79E-302	*Rpl36*	1.54E-259
Cpd	1.50E-192	*Selenop*	2.10E-295	*Rps16*	2.55E-258
C3	2.34E-187	*Lrp1*	2.08E-294	*Rpl24*	1.37E-257
Cxcl16	8.11E-183	*Lap3*	1.45E-290	*Rps9*	6.34E-253
Lgals3	1.57E-182	*Marcks*	2.77E-279	*Gpr141*	1.21E-246
Ube2j1	1.63E-180	*Glul*	3.64E-279	*Rpl27a*	3.06E-243
Plxnc1	9.84E-180	*Hebp1*	3.76E-278	*Rpl17*	8.15E-241
Stab1	4.07E-176	*Ear2*	4.53E-276	*Rps24*	1.46E-240
Cyth1	3.27E-163	*Apoc1*	2.49E-275	*Rps13*	2.34E-236
Spsb1	3.96E-163	*Kcna2*	3.72E-275	*Rpl38*	1.95E-226
Blnk	2.35E-162	*Myo10*	9.05E-269	*H2-DMb1*	1.02E-223
Cx3cr1	9.29E-162	*Atp13a2*	2.95E-267	*Rps18*	5.39E-223
Med10	5.25E-161	*Slc1a3*	6.24E-263	*Rpl19*	3.68E-221
Nek6	5.28E-160	*Slco2b1*	1.11E-258	*Rpl8*	2.01E-219
Ptms	1.05E-159	*mt-Nd2*	3.45E-258	*Rpl7a*	4.17E-217
Anxa5	1.10E-156	*Wwp1*	2.16E-253	*Gm34084*	5.23E-216
Gpnmb	1.21E-154	*Aplp2*	4.22E-248	*Rpl13*	2.08E-215
Itgb5	2.78E-154	*Atp8a1*	5.03E-248	*Rpl11*	2.47E-213
Myo5a	1.11E-146	*P2ry13*	3.17E-247	*Rpl35a*	2.13E-210
Runx3	1.81E-146	*Ccdc148*	4.70E-245	*Rpsa*	1.62E-209
Tmem176a	2.34E-144	*Grn*	1.58E-244	*Rpl6*	5.70E-208
Ctss	4.81E-141	*Bank1*	1.82E-239	*Tpt1*	2.63E-206
Sh3pxd2b	9.38E-141	*Mertk*	2.15E-238	*Rack1*	2.14E-203
Rtcb	4.42E-140	*Nr1h3*	1.13E-235	*Rpl23*	6.14E-199
Fam20c	1.91E-139	*Prnp*	2.93E-235	*Rpl26*	7.48E-198
Il2rg	8.84E-138	*Ninj1*	2.42E-234	*Rps6*	6.64E-197
Lpcat2	8.53E-137	*Fcna*	3.33E-233	*Rps10*	2.06E-195
Kynu	8.49E-136	*Csrp1*	1.16E-230	*Ier5*	1.06E-191
Tnfsf13b	8.77E-136	*Rgl1*	7.18E-229	*Rps3*	8.23E-185

Gpr157	1.18E-135	*Lpl*	4.94E-223	*Rpl27*	8.23E-185
Tgfbr1	7.63E-135	*Fam213b*	1.08E-222	*Rps5*	8.36E-185
H2-K1	1.15E-133	*Tcf7l2*	1.26E-222	*Rps7*	3.96E-182
Basp1	1.23E-133	*AB124611*	4.64E-221	*Rps15a*	6.82E-182
Pla2g7	1.80E-132	*Abcc3*	3.28E-216	*Rps11*	1.97E-180
Fth1	4.19E-131	*Fcgrt*	5.79E-216	*Rps4x*	5.07E-180
Ggh	1.85E-126	*Tgm2*	1.88E-215	*Rplp0*	3.09E-177
Adam19	6.94E-126	*Itgad*	5.35E-214	*Ly6i*	8.17E-176
C3ar1	7.35E-125	*Ptgs1*	2.94E-213	*S100a11*	6.23E-175
Ccl12	3.37E-123	*Laptm4a*	1.01E-212	*Atox1*	1.22E-174
Hvcn1	2.51E-121	*Comt*	1.33E-206	*Pim1*	9.56E-174
Anxa3	8.60E-121	*Creg1*	3.24E-205	*Sh3bgrl3*	3.97E-173
Tgfbi	1.88E-120	*Adgre1*	9.67E-205	*Ciita*	7.35E-173
Ctsd	2.73E-117	*Clec12a*	6.33E-204	*Eef1a1*	6.09E-172
Itm2c	5.19E-116	*Tspan4*	7.80E-203	*Rps3a1*	9.09E-168
Tmem119	5.62E-116	*Txn1*	9.13E-203	*Gm2a*	6.07E-165
Rap2a	1.03E-114	*Ctsb*	9.52E-201	*Ptprc*	2.05E-163
Ctsl	4.00E-114	*Mrap*	5.65E-197	*Rpl37*	1.51E-161
Itga6	1.83E-113	*Slc16a9*	5.99E-197	*Rps25*	3.03E-160
B4galnt1	2.45E-113	*Abcg3*	3.83E-196	*H3f3a*	5.92E-159
Fam3c	1.64E-112	*Pla2g15*	4.22E-196	*Btg2*	1.14E-158
Tmem173	1.54E-111	*C1qc*	6.17E-192	*Rpl15*	1.42E-158
Ski	3.59E-111	*Agpat3*	1.68E-191	*Cnn2*	1.09E-156
Anpep	5.85E-111	*Hs6st1*	1.95E-191	*Cdkn1a*	2.57E-156
Gng2	2.37E-110	*Dmpk*	2.15E-191	*Slfn1*	4.83E-155
Nceh1	2.88E-110	*Cd38*	1.79E-190	*Sem1*	4.08E-154
H2-Q7	4.94E-108	*Tmem26*	2.02E-189	*Lsp1*	1.34E-152
Rtn1	1.28E-106	*Slc11a1*	1.05E-188	*Rpl37a*	1.78E-152
Sorl1	1.31E-103	*Cd300a*	1.41E-187	*Rpl22*	3.64E-152
Glipr1	1.22E-102	*Slc7a7*	3.28E-187	*Sirpb1c*	4.81E-152
Gsn	2.00E-102	*Cyb5a*	6.94E-187	*Traf1*	6.97E-152
Afdn	4.54E-102	*Sipa1l1*	7.41E-187	*Emb*	4.22E-151
Ak2	1.11E-101	*Il18bp*	1.48E-186	*Rpl30*	1.32E-147
Ntpcr	2.21E-98	*Cd86*	2.52E-183	*Rps15*	1.14E-146
Scarb2	3.16E-97	*Vamp5*	3.05E-183	*H2-Ab1*	2.84E-145
Creb5	5.41E-97	*Jup*	6.69E-182	*Il1b*	3.05E-145
Gsto1	5.56E-97	*Blvra*	1.30E-178	*Rps28*	4.52E-145
Ncf1	4.26E-96	*Mgst1*	6.48E-178	*Jarid2*	1.82E-143
Ppfia4	4.97E-96	*Tbxas1*	1.47E-177	*Rps26*	1.53E-142
Chchd10	7.77E-96	*Hpgds*	2.04E-177	*Rpl32*	4.21E-142
Gna12	1.23E-95	*Tgfbr2*	2.70E-176	*Pld4*	9.07E-142
Mvb12b	1.80E-95	*Clec4n*	3.52E-175	*Cbfa2t3*	1.54E-141
Rasal3	1.45E-94	*Ms4a7*	5.30E-175	*Rps21*	4.04E-141

Scoc	6.86E-94	*Sirpa*	3.35E-171	*Fgr*	4.04E-141
Cfb	6.00E-93	*Fyn*	2.84E-168	*Rps8*	1.11E-139
Lmna	1.04E-92	*Cadm1*	2.20E-167	*Cd74*	5.34E-138

Table 2: List of the differentially expressed genes among *Timd4*$^{+}$ thymic macrophages, *Cx3cr1*$^{+}$ thymic macrophages, and thymic monocytes. The top 100 differentially expressed genes among the three clusters are listed by their negative $\log_{10}$ transformed p-value.